REVIEWS OF MODERN PHYSICS, VOLUME 96, OCTOBER–DECEMBER 2024

New developments in the numerical conformal bootstrap

Slava Rychkov

Institut des Hautes Études Scientifiques, 91440 Bures-sur-Yvette, France

Ning Su

Department of Physics, University of Pisa, I-56127 Pisa, Italy,
Walter Burke Institute for Theoretical Physics, California Institute of Technology, Pasadena, California 91125, USA,
and Department of Physics, Massachusetts Institute of Technology, Cambridge, Massachusetts 02139, USA

(published 21 November 2024)

Over the past 15 years, the numerical conformal bootstrap has become an indispensable tool for studying strongly coupled conformal field theories in various dimensions. Reviewed here are the main developments in the field in the five years since the publication of the previous comprehensive review [D. Poland, S. Rychkov, and A. Vichi, Rev. Mod. Phys. **91**, 015002 (2019)]. Developments in the software (`SDPB 2.0`, `scalar_blocks`, `blocks_3d`, `autoboot`, `hyperion`, and `simpleboot`) and on the algorithmic side (Delaunay triangulation, cutting surface, `tiptop`, navigator function, and `skydive`) are described. Also chronicled are the main physics applications that have been obtained using new technologies.

DOI: 10.1103/RevModPhys.96.045004

CONTENTS

I. INTRODUCTION

Conformal field theories (CFTs) are central to modern theoretical physics. They feature prominently as descriptions of continuous thermodynamic (Cardy, 1987) and quantum phase transitions (Sachdev, 2011), and of fixed points of renormalization group (RG) flows (Nakayama, 2015). They also play an important role in the study of the space of quantum field theories (Douglas, 2013), of string theory (Polchinski, 2007), of holographic approaches to quantum gravity (Aharony *et al.*, 2000), and of models of particle physics beyond the standard model (Luty and Okui, 2006). A main feature of CFTs is that their correlation functions can be defined nonperturbatively without explicit reference to a Lagrangian or any other microscopic description. Instead, the main dynamical principle of CFT is the operator product expansion (OPE) (Kadanoff, 1969; Wilson, 1969), which indicates that the local operators of the theory form an algebra under multiplication. Different CFTs are characterized by the spectrum of the local operators and by the OPE coefficients, which are the structure constants of the operator algebra. Possible OPE algebras are tightly constrained by the constraint of crossing symmetry: the correlation functions of the theory should be unambiguously defined regardless of the order in which one may decide to apply the OPE. The program of constraining or solving CFTs using this constraint, called the conformal bootstrap (Polyakov, 1974; Belavin, Polyakov, and Zamolodchikov, 1984), has experienced rapid development in the past 15 years.

In this review we focus on the numerical conformal bootstrap, which rewrites the constraint of crossing symmetry as a numerical problem to be solved on a computer[1] (Rattazzi *et al.*, 2008). The first ten years of the numerical conformal bootstrap were reviewed by Poland, Rychkov, and Vichi (2019).

Since then software and algorithmic advances have led to a marked increase in the sophistication of performed computations and a number of breakthroughs. Here we review these interesting recent developments. Our review is complementary to another recent review (Poland and Simmons-Duffin, 2022); however, we cover a larger number of topics and go more in depth in the description of the algorithms and the results.

We start by describing the developments in the software allowing the convex optimization, compute conformal blocks, and organize the computations to be performed (Sec. II). We then present a few physics results that were achieved only thanks to software developments (Sec. III). In Secs. IV–VIII we describe the main algorithmic developments (Delaunay triangulation, surface cutting, `tiptop`, the navigator function, and `skydive`), together with the physics results achieved thanks to them. We conclude in Sec. IX with prospects for future developments.

Our review is directed toward an audience that possesses some familiarity with the conformal bootstrap and its vocabulary. We advise others to see Poland, Rychkov, and Vichi (2019) before proceeding with our review.

II. SOFTWARE DEVELOPMENTS

The most important software development was the release of `SDPB 2.0` (Landry and Simmons-Duffin, 2019), a new version of the main bootstrap code `SDPB` (Simmons-Duffin, 2015). `SDPB` implements a primal-dual interior-point method for solving semidefinite programs (SDPs), taking advantage of sparsity patterns in matrices that arise in bootstrap problems and using arbitrary-precision arithmetic to deal with numerical instabilities when inverting poorly conditioned matrices.

The new version has improved the parallelization support. `SDPB 1.0` could run only on a single cluster node and used all cores of that node. `SDPB 2.0` can run on multiple cluster nodes with hundreds of cores. The speedup is proportional to the number of available cores. In addition, every core needs only some of the input data, which decreases the amount of required memory per node. Provided that one has access to a large cluster, `SDPB 2.0` can perform large computations that would take too long to complete with `SDPB 1.0` or would not fit on a single cluster node due to memory limitations.

A. Conformal blocks

To set up a bootstrap computation, one needs to precompute z and $\bar{z}$ derivatives of conformal blocks. Up to a prefactor they can be approximated by polynomials of the exchanged primary dimension. These polynomials are then processed using a framework software (see Sec. II.B) and passed to `SDPB`.

The simplest blocks are for the scalar external operators ("scalar blocks"). Many bootstrap studies have computed them using an algorithm from El-Showk *et al.* (2012, 2014b) that is implemented in *Mathematica*. This was limited by the number of *Mathematica* licenses available on the cluster. Recently, the algorithm was reimplemented as the fast open-source `C++` program `scalar_blocks` (Behan *et al.*, 2019). It computes scalar blocks in any spacetime dimension d, whether integer or noninteger.

Spinning external operators (such as fermions, conserved currents, and the stress tensor) are playing an increasingly important role in the bootstrap. Their conformal blocks are more complicated than scalar blocks. Spinning operator studies previously relied on *Mathematica* codes to compute the blocks. A `C++` program `blocks_3d` (Erramilli, Iliesiu, and Kravchuk, 2019; Erramilli *et al.*, 2021) has been released that computes $d = 3$ conformal blocks for external and exchanged operators of arbitrary spins.

B. Frameworks

A bootstrap framework is a software suite that, given problem specifications, generates CFT bootstrap equations, computes z and $\bar{z}$ derivatives of the crossing equation terms from the conformal block derivatives, generates `SDPB` input files, and launches and supervises `SDPB` computations. Several frameworks have been developed, the most powerful being `hyperion` (Simmons-Duffin, 2016) in `Haskell` and `simpleboot` (Su, 2019) in *Mathematica*, These frameworks also have support for `scalar_blocks`, `blocks_3d`, `SDPB 2.0`, and the algorithms discussed later (Delaunay triangulation, surface cutting, the navigator function, and `skydive`). Other frameworks include `JuliBootS` (Paulos, 2014) in `Julia` and `PyCFTBoot` (Behan, 2017) and `cboot` (Ohtsuki, 2016a) in `Python`.

For CFTs with global symmetry, the bootstrap equations involve the crossing kernels ($6j$ symbols) of the group. For finite groups and Lie groups with a small number of generators, `autoboot` (Go and Tachikawa, 2019; Go, 2020) is a package designed to automate the derivation of the crossing kernel and produce bootstrap equations for scalar correlators. The package uses `cboot` as a framework software to launch `SDPB`. The framework `simpleboot` can also work with the bootstrap equations produced by `autoboot`.

III. PUSHING THE OLD METHOD

From 2015 to 2020, numerical bootstrap studies were performed mostly using the following approach (Kos, Poland, and Simmons-Duffin, 2014a; Simmons-Duffin, 2015). The bootstrap equations are truncated by taking the derivatives at the crossing symmetric point. Derivatives of the conformal block are approximated by polynomials up to a positive prefactor. Together with certain assumptions on CFT data, the bootstrap equation is translated into an SDP problem. The SDP is solved in the "feasibility mode" to determine whether the assumptions are allowed or disallowed. Parameters of the theory space are scanned over using bisection or the

[1] See Bissi, Sinha, and Zhou (2022) and Hartman *et al.* (2022) for reviews of parallel developments in the analytic conformal bootstrap.

Delaunay search; see Sec. IV.A. With this method (referred to in this review as the old method), the number of parameters usually cannot be too large. However, many interesting results have been produced in the past few years using this method, thanks especially to the software developments described in Sec. II. In this section we review some of those results. Most computations in this section used `SDPB 2.0` to solve SDPs, and would not have been possible with `SDPB 1.0`.

A. 3D $\mathcal{N} = 1$ supersymmetric Ising CFT

The Gross-Neveu-Yukawa model with one Majorana spinor is described by the following Lagrangian:

$$\mathcal{L} = \frac{1}{2}(\partial_\mu \sigma)^2 + m^2\sigma^2 + \bar{\psi}\partial\!\!\!/\psi + \frac{\lambda_1}{2}\sigma\bar{\psi}\psi + \frac{\lambda_2^2}{8}\sigma^4, \qquad (1)$$

where ψ is a three-dimensional Majorana spinor. The Lagrangian is invariant under the time-reversal symmetry (T parity) where $\sigma \to -\sigma$ and $\psi \to \gamma^0\psi$. In the UV regime when $\lambda_1 = \lambda_2$ and $m = 0$, the model becomes an $\mathcal{N} = 1$ supersymmetry (SUSY) Wess-Zumino model with superpotential $\mathcal{W} = \lambda\Sigma^3$ and $\Sigma = \sigma + \bar{\theta}\psi + (1/2)\bar{\theta}\theta\epsilon$. For a particular value of the mass term m^2, the model flows in the IR to a fixed point referred to as the 3D $\mathcal{N} = 1$ SUSY Ising CFT. The SUSY is explicitly broken for generic values $\lambda_1 \neq \lambda_2$. However, the SUSY could emerge in the IR theory from a nonsupersymmetric system by tuning a single macroscopic parameter, provided that there is only one relevant singlet under T parity (Grover, Sheng, and Vishwanath, 2014). Grover, Sheng, and Vishwanath (2014) argued that this fixed point might be realized as a quantum critical point at the boundary of a $(3+1)$D topological superconductor.

The 3D $\mathcal{N} = 1$ SUSY Ising CFT was first studied via bootstrap techniques using a single correlator of a scalar (Bashkirov, 2013) or a fermion (Iliesiu *et al.*, 2016); see Poland, Rychkov, and Vichi (2019) for a review. Later Atanasov, Hillman, and Poland (2018) and Rong and Su (2021b) extended the analysis to correlators involving σ and ϵ. From a non-SUSY point of view, the bootstrap setup is the same as the 3D Ising σ, ϵ setup of Kos, Poland, and Simmons-Duffin (2014a), who realized $\mathbb{Z}_2$ through T parity. Supersymmetry imposes the additional constraints $\Delta_\epsilon = \Delta_\sigma + 1$ since σ and ϵ are in the same supermultiplet, and the OPE coefficients $\lambda_{\sigma\sigma O}$, $\lambda_{\epsilon\epsilon O}$ are related to $\lambda_{\sigma\epsilon P}$, where O and P belong to the same supermultiplet. Rong and Su (2021b) thoroughly worked out those constraints and injected them into the σ, ϵ setup. By demanding that under T parity only one even scalar operator and two odd scalar operators are relevant, Rong and Su (2021b) isolated the CFT as a small island in the theory space and produced precise critical exponents with rigorous error bars[2]: $\eta_\sigma = 0.168\,888(\mathbf{60})$ and $\omega = 0.882(\mathbf{9})$. This provides strong evidence that the theory has superconformal symmetry and has only one relevant singlet under T parity, confirming the possibility of emergent supersymmetry.

TABLE I. Results of Atanasov *et al.* (2022) for the scaling dimensions of the leading parity-odd scalars σ and σ' in the 3D $\mathcal{N} = 1$ super-Ising model. The uncertainties in boldface are rigorous.

CFT data	Critical exponents
$\Delta_\sigma = 0.584\,443\,5(\mathbf{83})$	$\eta_\sigma = \eta_\psi = 0.168\,887(\mathbf{17})$ $1/\nu = 1.415\,557(\mathbf{8})$
$\Delta_{\sigma'} = 2.8869(\mathbf{25})$	$\omega = 0.8869(\mathbf{25})$

There are two follow-up works (Rong and Su, 2021a; Atanasov *et al.*, 2022). As of 2023 the most precise conformal data for this CFT were obtained from Atanasov *et al.* (2022) using the same setup as Rong and Su (2021b), but at a much higher $\Lambda = 59$. The computation at such a high Λ becomes feasibly practical by utilizing `scalar_blocks` and `SDPB 2.0`. The result is summarized[3] in Table I and Fig. 1.

Rong and Su (2021a) studied more general $\mathcal{N} = 1$ Wess-Zumino models with global symmetries, obtaining strong bounds on CFT data. However, no small bootstrap islands have been identified. The bootstrapping of generic SUSY Wess-Zumino models remains a challenging task.

B. Bootstrapping critical gauge theories

An important class of CFTs is critical gauge theories, i.e., the IR fixed point of Abelian or nonabelian gauge fields coupled to matter fields. The simplest examples are fermionic and bosonic 3D quantum electrodynamics (QED_3), where N_f Dirac fermions or complex bosons are coupled to the $\mathrm{U}(1)$ gauge field. In both cases the theories are believed to flow to an IR CFT at large N_f, while in the small N_f cases, they might not be critical. Determining the precise extent of the conformal window of these theories (i.e., the range of N_f when they flow to an IR fixed point) presents a long-standing problem.[4] Moreover, these models have a rich connection to the deconfined quantum critical point (DQCP) (Senthil, Balents *et al.*, 2004; Senthil, Vishwanath *et al.*, 2004) and Dirac spin liquid (Hermele, Senthil, and Fisher, 2005; Song *et al.*, 2019, 2020) in condensed matter physics.

Critical gauge theories present interesting targets for the conformal bootstrap. Previously monopole operators in fermionic QED_3 were studied via the bootstrap discussed by Chester and Pufu (2016) and Chester *et al.* (2018). Various bootstrap bounds for bosonic QED_3 were obtained by Nakayama and Ohtsuki (2016), Iliesiu (2018), and Li (2022b), who offered insights into the nature of DQCP; see also Poland, Rychkov, and Vichi (2019) and Poland and

[2]Prior to this work, the best estimates of those critical exponents were $\eta_\sigma = 0.170$ and $\omega = 0.838$, which were obtained from the four-loop ϵ expansion of the Gross-Neveu-Yukawa model (Zerf *et al.*, 2017). Owing to the sign problem, there is no Monte Carlo simulation for this model.

[3]The relations between the scaling dimensions and the critical exponents are as follows: $\eta_\sigma = 2\Delta_\sigma + 1$; $1/\nu = 1 - \Delta_\epsilon$, where $\Delta_\epsilon = \Delta_\sigma + 1$; and $\omega = \Delta_{\epsilon'} - 3$, where ϵ' is the leading irrelevant singlet. In the present case ϵ' is the bosonic descendant of σ', and $\Delta_{\epsilon'} = \Delta_{\sigma'} + 1$.

[4]See Gukov (2017) for a survey of approaches to the conformal window problem for the fermionic QED_3.

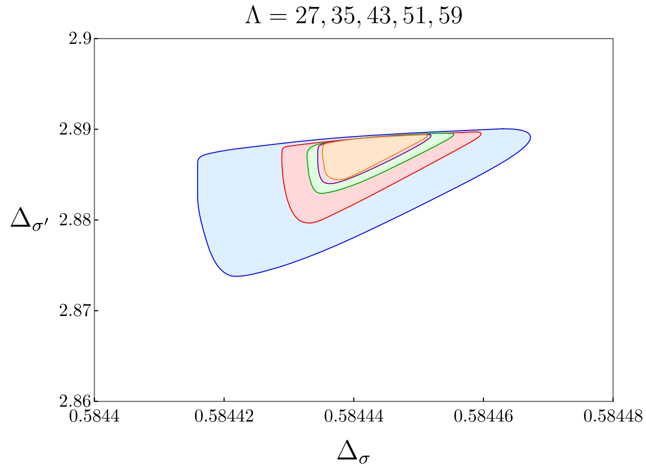

FIG. 1. Allowed region from Atanasov *et al.* (2022) for the scaling dimensions of the leading parity-odd scalars σ and σ' in the 3D $\mathcal{N} = 1$ super-Ising model.

Simmons-Duffin (2022) for a review. In this section we discuss more recent progress, focusing on 3D nonsupersymmetric theories.[5]

Critical gauge theories are generally more difficult to bootstrap than the fixed points of scalar theories, like the $O(N)$ model. One difficulty arises because the fundamental matter field is charged under the gauge group, and hence their correlation functions are not good CFT observables. Gauge-invariant operators are built out of products of fundamental fields and have a higher scaling dimension, while the numerical bootstrap is known to converge slower when operators of higher scaling dimensions are involved. Because of this and other difficulties, small bootstrap islands have not yet been obtained for even the simplest critical gauge theories. New ideas may be needed, such as bootstrapping correlators of closed or open Wilson lines. It is not now clear how to effectively bootstrap these objects. We later discuss works that bootstrapped correlators of gauge-invariant operators using the "old method."

The global symmetries of QED_3 are the $SU(N_f)$ flavor symmetry of the matter sectors, as well as the topological $U(1)$ symmetry. The monopole operators carry a nonzero charge q under $U(1)$, and their specific representation under $SU(N_f)$ depends on q, N_f, and whether the matter sector is bosonic or fermionic. Therefore, the bootstrap equations involving monopoles are different for bosonic and fermionic QED_3. In Secs. III.B.1 and III.B.2, we discuss the bootstrap studies of scalar correlators in fermionic and bosonic QED_3, respectively. In Sec. III.B.3 we discuss bootstrap studies of the correlator of flavor currents. This setup applies to all CFTs with a flavor current.

1. Bootstrapping fermionic QED_3

Fermionic QED_3 at large N_f is believed to flow to a CFT with a global symmetry $G_{\mathrm{IR}} = SU(N_f) \times U(1)$ in the IR, where $SU(N_f)$ is the flavor symmetry of the four Dirac fermions and $U(1)$ is the flux conservation symmetry of the gauge field. At small $N_f < N_{\mathrm{crit}}$ the IR theory is in a chiral symmetry breaking phase. The specific value of N_{crit} has been studied with many different methods, yet there is no consensus (Gukov, 2017).

The $N_f = 4$ case is particularly interesting. If the $N_f = 4$ case is indeed conformal, several lattice models and materials, including the spin-$1/2$ Heisenberg model on the kagome and triangular lattices, are conjectured to realize it as a critical conformal phase (He *et al.*, 2017; Hu *et al.*, 2019). The UV lattice models usually possess a symmetry G_{UV} that is smaller than G_{IR}. For the fixed point to be reached, i.e., for the conformal phase to be realized in those lattice models, all G_{UV} singlet operators (which includes G_{IR} singlets but also some operators charged under G_{IR}) have to be irrelevant. Therefore, the fate of those lattice models depends on the precise spectrum data of the IR CFT.

Specifically, the topological charge $q = 1$ monopole operator M_1 and a charge neutral operator[6] $S_{(220)}$ must be irrelevant for the conformal phase scenario to be realized in the kagome lattice (Song *et al.*, 2019, 2020). QED_3 has been studied using both large-N_f expansion and Monte Carlo simulations. While Monte Carlo simulations support the CFT scenario (Karthik and Narayanan, 2016a, 2016b, 2019), large-N predictions yield $\Delta_{M_1} \approx 2.499$ and $\Delta_{S_{(220)}} \approx 2.379$ (Chester and Pufu, 2016), which are relevant and would rule out the CFT scenario on the kagome lattice.

The bootstrap study of a single correlator of the fermion bilinear operator was initiated by Li (2022a), who injected various large-N expansion results into the setup. They observed a kink moving with the dimension Δ_* of the first scalar in a certain representation [denoted as $T\bar{A}$ by Li (2022a)] and suggested that the kink may correspond to the fermionic QED_3 if Δ_* is fixed to the actual CFT value.

Two subsequent bootstrap studies (Albayrak *et al.*, 2022; He, Rong, and Su, 2022) investigated the mixed correlators between the lowest monopole and the fermion bilinears. Strong bounds on CFT data have been obtained; see Fig. 2. He, Rong, and Su (2022) imposed gap assumptions that are compatible with the conformal phase scenarios (specifically, $\Delta_{M_1} \geq 3$ and $\Delta_{S_{(220)}} \geq 3$ for the kagome lattice). The resulting bounds are consistent with the latest Monte Carlo results but excluded certain results from large N_f expansion. However, Albayrak *et al.* (2022) imposed various gap assumptions inspired by the large-N_f result. Specifically, they assumed that $\Delta_{M_1} \leq 2.6$ and $\Delta_{S_{(220)}} \geq 2.8$. They found bounds in an isolated region compatible with the large-N prediction. Albayrak *et al.* also introduced a useful technique called interval positivity to implement gap assumptions of the form $\Delta_{\min} \leq \Delta \leq \Delta_{\max}$. In both works the relevance of M_1 and $S_{(220)}$ is not determined by a bootstrap computation

[5]See Chester and Pufu (2016) and Chester *et al.* (2018) for discussions of progress on 4D critical gauge theories.

[6]Here (abc) denotes the Young diagram of the representation. Both M_1 and $S_{(220)}$ transforms as (220) under $SU(4)$. He, Rong, and Su (2022) referred to M_1 as $M_{4\pi}$ or (T, T) and called S_{220} (T, S), where T and S refer to the traceless symmetric tensor and singlet in $O(6) \times O(2) \approx SU(N_f) \times U(1)$.

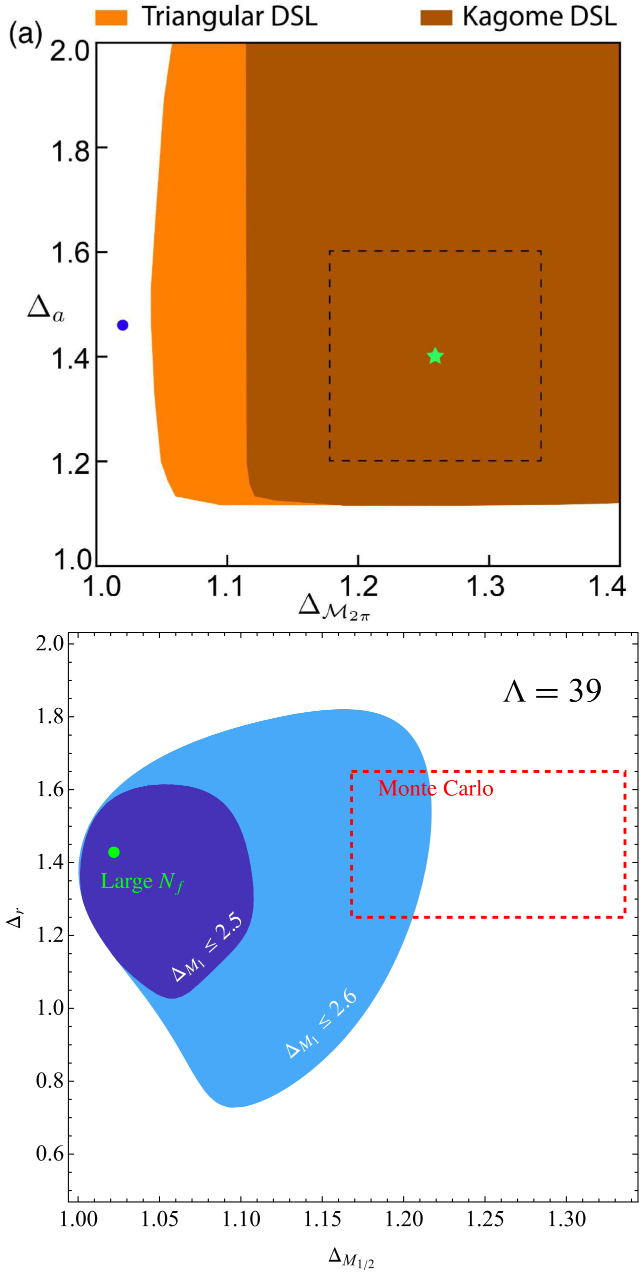

FIG. 2. Top panel: the allowed region in the space of dimensions of the fermion bilinear (a) and the monopole ($\mathcal{M}_{2\pi}$) of He, Rong, and Su (2022). The gap assumptions are imposed to be compatible with the conformal phase scenario on the triangular lattice and the kagome lattice. The green (light gray) star and the dashed error box represent the results of a Monte Carlo simulation, while the blue point is from the large-N_f expansion. Bottom panel: the allowed region in the space of dimensions of the fermion bilinear (Δ_r) and the monopole ($\mathcal{M}_1$) of Albayrak *et al.* (2022). The green (light gray) dot indicates the result from the large-N_f expansion, while the red dashed box is from a Monte Carlo simulation. See Albayrak *et al.* (2022) for details.

but instead input as an assumption, and a reliable spectrum has not been obtained. Thus, the matter cannot be considered settled.

In the $N_f = 2$ case Li (2022b) bootstrapped the correlator of the lowest monopole operator. When the constraints of RG stability and/or the O(4) symmetry enhancement (Xu and You, 2015) were imposed, the bounds of Li (2022b) were confronted with determinations of scaling dimensions in Monte Carlo simulations, which is inconsistent with the results of Qin *et al.* (2017) but marginally consistent with the findings of Karthik and Narayanan (2016b, 2019).

2. Bootstrapping bosonic QED$_3$

Several works have bootstrapped the bosonic QED$_3$. One issue is how to distinguish QED$_3$ from non-Abelian SU(N_c) gauge theories with the same number of matter field multiplets. This question was investigated by He, Rong, and Su (2021a) and Reehorst, Refinetti, and Vichi (2023). The key observation is that there are natural gaps in the spectrum that distinguish between different N_c values. The simplest example concerns an operator of the form $\bar{\phi}^{[f_1}_{[c_1}\bar{\phi}^{f_2]}_{c_2]}\phi^{[c_1}_{[f_3}\phi^{c_2]}_{f_4]}$, where ϕ are the bosonic matter fields in the fundamental of SU(N_c) and f_i and c_i are the flavor and color indices, respectively. This operator exists when $N_c \geq 2$, but an operator transforming in the same way under the global symmetry cannot be constructed in the Abelian cases when using just four scalars without derivatives. Thus, imposing a gap in this symmetry sector could in principle isolate the Abelian case from $N_c \geq 2$. With such a gap assumption, He, Rong, and Su (2021a) bootstrapped the correlator of the leading scalar in SU(N_f) adjoint and found bounds in a closed region for the large-N_f cases and in $(2+\epsilon)$D for small-N_f cases. However, it is not clear whether the closed region contains only the target theory or whether it could converge to a small bootstrap island at large Λ and produce a precise scalar QED spectrum.

The $N_f = 2$ case is believed to be the simplest example of the DQCP. The Monte Carlo simulations are in tension with the bootstrap bounds; see Poland, Rychkov, and Vichi (2019) for a review. A possible way to reconcile the bootstrap results with the Monte Carlo simulations was proposed by Ma and Wang (2020) and Nahum (2020). They suggested a formal interpolation between the 2D SU$(2)_{k=1}$ Wess-Zumino-Witten (WZW) theory and the 3D DQCP. With a one-loop calculation, they found the critical dimension $d_c \approx 2.77$, where the theory annihilates with another fixed point and becomes a pair of complex CFTs, which is an example of the merger and annihilation scenario (Gorbenko, Rychkov, and Zan, 2018a, 2018b). If this scenario is correct, the bosonic QED$_3$ for $N_f = 2$ does not exist in three dimensions as a unitary fixed point, and the DQCP phase transition is first order, but only weakly so since the RG flow passes a long time flowing between a pair of complex CFTs, behavior referred to as walking.

This scenario may be checked via the numerical bootstrap analysis of the SU$(2)_{k=1}$ WZW theory in two dimensions and in noninteger $d > 2$. The first 2D analysis was performed by Ohtsuki (2016b), who discovered that the WZW theory sits at a sharp kink of a single-correlator bound. Then He, Rong, and Su (2021b) and Li and Poland (2021) investigated the fate of this kink in noninteger $d > 2$, as well as in the case of larger N_f. He, Rong, and Su (2021b) found evidence to support the critical dimension proposed by Ma and Wang (2020).

In spite of these developments, the puzzle of DQCP cannot be considered fully clarified. Recently, evidence has emerged from Monte Carlo (Takahashi *et al.*, 2024) and from the calculations on the fuzzy sphere[7] (Chen *et al.*, 2023; Chen, Zhang, and Meng, 2024) that the phase transition is weakly first order due to a tricritical point, a scenario more mundane than complex CFT (walking), but previously deemed unlikely to require tunings in the microscopic models. [At the same time, another fuzzy sphere calculation (Zhou *et al.*, 2024) argued for consistency with the walking scenario.] The tricritical scenario was considered in a bootstrap study using more modern techniques (Chester and Su, 2024); see Sec. VII.B.

3. Bootstrapping the flavor currents

The existence of conserved currents is a key feature of all local CFTs possessing continuous global symmetry. Global symmetry currents (hereafter referred to simply as currents) are CFT primaries of spin 1 that are conserved and have the protected scaling dimension $d-1$. In addition, OPE coefficients of currents with other primaries are constrained by Ward identities. Implementing those properties in a bootstrap setup could lead to new bounds and new spectral data that cannot be accessed in setups dealing only with scalar primaries.

For the problem of bootstrapping critical gauge theories, correlators involving currents are appealing to consider for several other reasons. For Abelian gauge theories in three dimensions, the existence of the topological current $j^\rho_{\rm top} = \epsilon^{\mu\nu\rho}\partial_\mu A_\nu$ is a key feature; operators charged under this current are called monopole operators. The existence of this current could distinguish fermionic QED_3 from the free fermion theory. Later in the review we see other examples of how correlators of currents can help distinguish critical gauge theories from other theories.

The bootstrap study of the four-point function of currents in 3D CFTs with a $\mathrm{U}(1)$ symmetry was initiated by Dymarsky *et al.* (2019). Subsequently, Reehorst, Trevisani, and Vichi (2020) studied the 3D $\mathrm{O}(2)$ model using mixed correlators of the $\mathrm{O}(2)$ current and a singlet. Reehorst, Trevisani, and Vichi (2020) obtained several pieces of new data that were not accessible in prior scalar correlator studies of the $\mathrm{O}(2)$ model (Kos, Poland, and Simmons-Duffin, 2014b), although Reehorst, Trevisani, and Vichi (2020) used some results of Kos, Poland, and Simmons-Duffin (2014b) as an input. As mentioned, Abelian 3D gauge theories have $\mathrm{U}(1)$ topological currents. However, no features associated with these theories were observed in the bounds of Dymarsky *et al.* (2019) or Reehorst, Trevisani, and Vichi (2020).

More recently He *et al.* (2023) bootstrapped for the first time the four-point functions of currents in the CFTs with a non-Abelian continuous symmetry. As in the bosonic QED case studied by He, Rong, and Su (2021a), He *et al.* (2023) proposed to impose gap assumptions on the spectrum of exchanged operators, which can be used to distinguish between different N_c for the fermionic case and, in particular, the Abelian from the non-Abelian cases. In fermionic $\mathrm{U}(N_c)$ gauge theories, consider an operator of the form $\bar\psi^{(f_1,c_1}\gamma^\mu\psi_{(f_2,c_1}\bar\psi^{f_3,c_2)}\gamma^\nu\psi_{f_4,c_2)}$, where f_i and c_i denote the flavor and color indices, respectively, and the parentheses symmetrize the f_i flavor indices. This operator exists only for $N_c \geq 2$ and has a scaling dimension of 4 in the large-N_f limit. Thus, a gap beyond 4 in this channel could in principle distinguish fermionic QED from fermionic QCD. The representation to which this operator

[7]A novel numerical method proposed by Zhu *et al.* (2023).

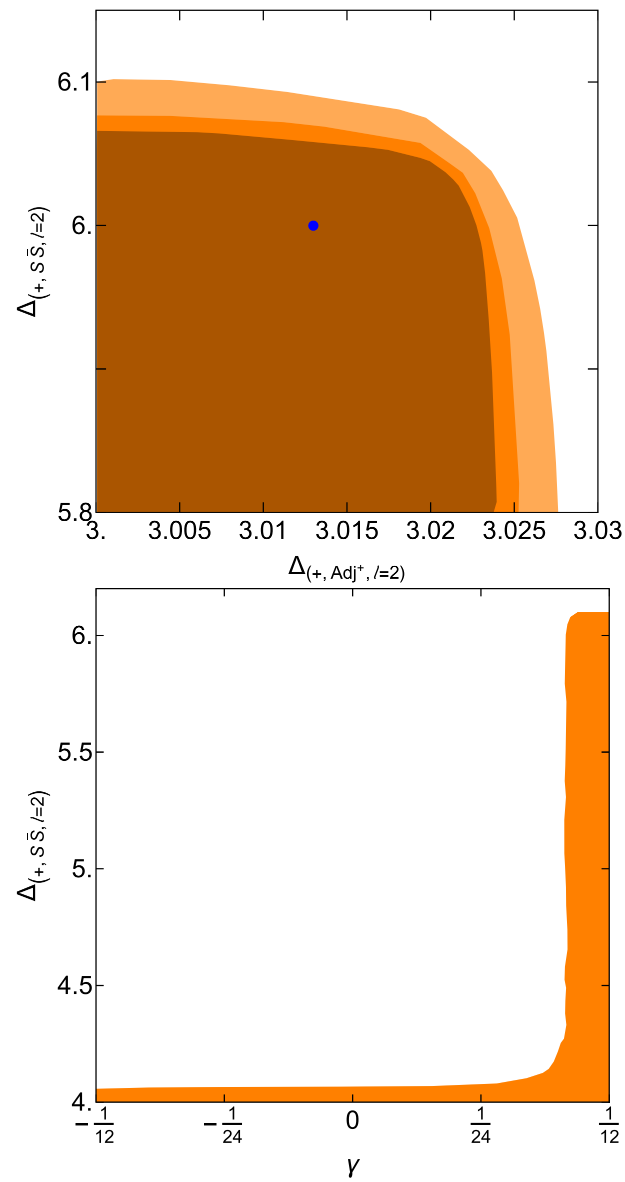

FIG. 3. Feasibility bounds from bootstrapping non-Abelian currents. Top panel: the lowest operator in the $(+, S\bar{S}, \ell = 2)$ sector vs the sector $(+, \mathrm{Adj}^+, \ell = 2)$ in $\mathrm{SU}(100)$ CFT, where Adj^+ is the adjoint representation. The light, medium, and dark orange bounds are for $\Lambda = 19$, 23, and 27, respectively. The blue (dark gray) dot is the large-N result. Bottom panel: γ vs the lowest operator in the $(+, S\bar{S}, \ell = 2)$ sector in $\mathrm{SU}(100)$ CFT. $\Lambda = 19$. γ is a parameter appearing in the current-current-stress tensor three-point function that obeys the conformal collider bounds $|\gamma| \leq 1/2$ (Hofman and Maldacena, 2008). In both cases, mild gaps in several sectors are imposed. The bounds are insensitive to those gap assumptions. From He *et al.*, 2023.

belongs was denoted by He et al. (2023) as $(+, S\bar{S}, \ell = 2)$, where $+$ denotes the spacetime parity and ℓ is the spin. This gap could also remove the solution of the generalized free field (GFF), where the leading operator $(J^\mu)^{(f_1}{}_{(f_2}(J^\nu)^{f_3)}{}_{f_4)}$ has the scaling dimension 4. Note that $(+, S\bar{S}, \ell = 2)$ was previously accessed in the scalar bootstrap of Albayrak et al. (2022) and He, Rong, and Su (2022). However, in that setup the GFF operator[8] has a scaling dimension of 6. Indeed, He, Rong, and Su (2022) found no signal of $N_f = 4$ QED$_3$ in this sector. We see a clear advantage of the setup involving external currents.

By scanning over the gaps in $(+, S\bar{S}, \ell = 2)$ and other parameters, He et al. (2023) obtained strong bounds on CFT data and observed kinks; see Fig. 3. Large-N_f QED$_3$ appears to be close to some kinks. He et al. (2023) also imposed stronger conditions by demanding that many operators lie within mild windows around the large-N_f values. With such assumptions in large N_f cases, the bound turns into an isolated region that does not contain any obvious known theories other than $N_f = 4$ QED$_3$. However, the isolated region is not small enough to produce a precise QED spectrum. Furthermore, it is not clear whether the closed regions could converge to a small bootstrap island at high Λ.

The discussed recent computations were allowed by the progress in the conformal block and SDP software. In the first U(1) current study of Dymarsky et al. (2019), the conformal blocks of the current correlator were computed by decomposing them into derivatives of scalar blocks. However, the setup of He et al. (2023) produced SDPs that are much larger in size than those of Dymarsky et al. (2019) and are more challenging to generate and compute. These calculations have become feasible due to the development of `blocks_3d` and `SDPB 2.0`, as discussed in Sec. II.

To summarize, bootstrapping critical gauge theories remains a challenge. Various attempts to bootstrap QED in three dimensions and $(2+\epsilon)D$) have been made. Despite having found strong bounds in the theory space, no one has obtained a small bootstrap island that could produce precise and reliable CFT data. In future work for a successful bootstrap analysis of QED, it might be necessary to consider larger systems of mixed correlators. One could also consider correlators involving open or closed Wilson lines, although formulating a conformal bootstrap program for these observables is an open problem.

C. Multiscalar CFTs

In this review by a multiscalar CFT we mean an IR fixed point of a Lagrangian field theory of N scalar fields with quartic interactions in the UV, which respect the global symmetry $G \subset O(N)$. Physically one is most interested in stable fixed points, i.e., possessing only one relevant singlet scalar (the mass term). For small N the possible stable fixed points are limited. See Rong and Rychkov (2023) for a classification of all stable fixed points for up to five scalars based on one-loop calculations in $d = 4 - \epsilon$ dimensions. Apart from the Ising and O(N) CFTs, simple multiscalar CFTs include those with symmetries $\mathbb{Z}_2^n \rtimes \mathcal{S}_n$ (the cubic symmetry), $\mathbb{Z}_2 \times \mathcal{S}_n$, $O(m)^n \rtimes \mathcal{S}_n$, and $O(m) \times O(n)$. For all of these symmetry groups there exists a family of d-dimensional CFTs that for $d = 4 - \epsilon$ and $\epsilon \ll 1$ is weakly coupled and smoothly connects to the free theory for $d = 4$. These families can be studied via the ϵ expansion, which, when extended for $\epsilon = 1$ and Borel resummed, gives predictions for 3D CFTs. Several works have studied CFTs with these global symmetries using the conformal bootstrap. One hope for these studies is to recover the results predicted via the ϵ expansion using the nonperturbative technique (perhaps with a better precision). In addition, one may hope to discover other CFTs having the same global symmetry (in addition to the one predicted by the ϵ expansion).

Bootstrap studies of CFTs with the cubic symmetry $\mathbb{Z}_2^n \rtimes \mathcal{S}_n$ began with Rong and Su (2018) and Stergiou (2018). Bounds from a single correlator of an operator v in the standard n-dimensional representation have been obtained during work in three dimensions. While some kinks were observed on the bounds, they do not correspond to the "cubic CFT," i.e., the CFT predicted by the ϵ expansion (Aharony, 1973). Stergiou (2018) conjectured that the kink corresponds to a new CFT that they called the Platonic CFT.[9] Kousvos and Stergiou (2019, 2020) further investigated the conjectured platonic CFT by examining four-point functions involving v and one additional operator. With certain gap assumptions they constrained the theory to an isolated region.

Nakayama and Ohtsuki (2014) and Henriksson, Kousvos, and Stergiou (2020) studied theories with $O(m) \times O(n)$ symmetry. Kinks were observed on the bounds from a single correlator of ϕ_{ar} [the bifundamental representation, with a and r being the O(m) and O(n) vector indices, respectively], and they are consistent with the large-n expansion for $O(m) \times O(n)$ Wilson-Fisher theories at fixed m. Using a mixed correlator setup involving ϕ_{ar} and the leading singlet operator, Henriksson, Kousvos, and Stergiou (2020) showed that the CFT can be constrained to an isolated region by demanding that a certain operator saturate a bound.

Similar methods were applied to the $O(m)^n \rtimes \mathcal{S}_n$ symmetry (Stergiou, 2019; Henriksson and Stergiou, 2021; Kousvos and Stergiou, 2022) and the $U(m) \times U(n)$ symmetry (Kousvos and Stergiou, 2023). Stergiou (2019) studied a single correlator of ϕ_i, where $i = 1, \ldots, mn$ labels n copies of O(m) vectors transforming under $O(m)^n \rtimes \mathcal{S}_n$. Focusing on the $O(2)^2 \rtimes \mathcal{S}_2$ case, Stergiou (2019) made interesting observations: several materials are supposed to undergo phase transitions described by a CFT with $O(2)^2 \rtimes \mathcal{S}_2$. Experiments on these phase transitions have yielded two sets of critical exponents. Surprisingly two kinks were exhibited on the single-correlator bound, which is in good agreement with the two sets of experimental data. Henriksson and Stergiou

[8]To construct a spin-2 operator using scalar operators, two derivatives have to be inserted.

[9]Stergiou (2018) provided evidence that the Platonic CFT exists and is distinct from the cubic CFT, not only in $d = 3$ but also in $d = 3.8$. However, from recent work (Rong and Rychkov, 2023) near $d = 4$ and with up to five scalars, we do not expect other weakly coupled theories, apart from the cubic CFT, to exhibit cubic symmetry. This suggests that the Platonic CFT might have a larger symmetry and its Lagrangian description may involve more than five scalar fields. It would be worthwhile to clarify this issue.

(2021) further studied the kinks at the large-m limit. Kousvos and Stergiou (2022) investigated a mixed correlator system involving ϕ and an operator X that is a singlet under $\mathrm{O}(m)$ but a fundamental representation in $\mathcal{S}_n$. Kousvos and Stergiou (2022) found isolated regions under certain gap assumptions. However, the fate of the two possible $\mathrm{O}(m)^n \rtimes \mathcal{S}_n$ CFTs remains undetermined.

In conclusion, despite obtaining many strong bounds for various multiscalar CFTs, small bootstrap islands have still not yet been obtained for those theories. Reehorst and Sirois (2023) and Reehorst *et al.* (2024) achieved this for the multiscalar CFTs with $\mathrm{O}(N) \times \mathrm{O}(2)$ global symmetry. Outside the scope of local theories, Behan (2019) studied all three relevant scalars in the long-range Ising model and found a kink in the numerical bounds that corresponds to the target CFT; further interesting results for this model were obtained by Behan *et al.* (2023).

D. Extraordinary phase transition in the O(N) boundary CFT

Conformal defects are difficult to bootstrap using the rigorous numerical conformal bootstrap methods based on SDPs since the OPE coefficients in the bootstrap equation involving both the bulk and the defects generally do not exhibit positivity properties. One nonrigorous approach usually applied to bootstrap these systems is Gliozzi's method (Gliozzi, 2013), where one directly solves the truncated bootstrap equation without assuming positivity of the OPE coefficients. However, the error in this method is not systematically controllable.

In this section we review a recent exploration (Padayasi *et al.*, 2022) of bootstrapping the boundary of 3D $\mathrm{O}(N)$ CFTs that represents a special case in which the standard SDP approach can be applied. The system under consideration is the Heisenberg model on a d-dimensional lattice with an infinite plane boundary at $x_d = 0$,

$$\mathcal{H} = -\sum_{\langle i,j \rangle} K_{i,j} \vec{S}_i \cdot \vec{S}_j, \tag{2}$$

where $\vec{S}_i$ is the classical $\mathrm{O}(N)$ spin, $\langle i, j\rangle$ denotes a pair of neighboring sites, $K_{i,j} = K_1$ when the pair is on the boundary, and $K_{i,j} = K$ when the pair is in the bulk. Depending on N, the system exhibits different properties. An extraordinary-log[10] boundary transition happens when $2 \le N \le N_c$ (Metlitski, 2022). N_c is determined by parameters that can be extracted by studying another boundary universality class, called the normal transition, where an ordering field is applied on the boundary. At the normal transition, the crossing equation (bulk-to-boundary bootstrap equation) for the two-point function of real scalars is schematically

$$1 + \sum_k \lambda_k f_{\mathrm{bulk}}(\Delta_k, \xi) = \xi^{\Delta_\phi} \left(\mu_\phi + \sum_n \mu_n f_{\mathrm{bry}}(\hat{\Delta}_n, \xi) \right), \tag{3}$$

where $\sum_k$ is over the bulk operator and ξ is a bulk-boundary cross ratio; $\sum_n$ is the sum over the boundary operators. In the case of $\mathrm{O}(N)$ CFT, these terms are dressed with the $\mathrm{O}(N)$ tensor structure, which contains N explicitly. Then certain OPE coefficients determine N_c. Specifically, the extraordinary-log phase transition happens when the quantity $\alpha = (1/32\pi)(\mu_\sigma/\mu_t) - (N-2)/2\pi$ is positive, where μ_t and μ_σ are OPE coefficients.

The OPE coefficients in Eq. (3) are generally not positive. However, in this case the $2+\epsilon$, large-N, and $4-\epsilon$ calculations all show that these coefficients are positive. Padayasi *et al.* (2022) studied the system using Gliozzi's method, which showed no negativity for those OPE coefficients. They then assumed the positivity of coefficients and formulated the problem as an SDP. They applied the standard approach to map out the feasible region in α vs N. Padayasi *et al.* found the bound $N_c > 3$, which is rigorous if one accepts the positivity assumptions. With the Gliozzi method they found that $N_c \approx 4$, which is consistent with the Monte Carlo results. Their work is an example in which the standard SDP method could be applied to study the bulk-to-boundary bootstrap equation in certain situations.

IV. DELAUNAY TRIANGULATION AND SURFACE CUTTING

Incorporating more and more crossing equations should increase the constraining power of the conformal bootstrap. This was demonstrated by Kos, Poland, and Simmons-Duffin (2014a) and Kos *et al.* (2015, 2016), who used more than one crossing equation for the first time. Furthermore, Kos *et al.* (2016) showed that the nondegeneracy of an isolated exchanged operator is a powerful constraint. This isolated nondegenerate operator may be one of the external operators or an operator that is otherwise known to be nondegenerate. When the nondegeneracy condition is imposed, the contribution of an isolated operator to a crossing equation is proportional to a rank-1 positive-semidefinite matrix that is parametrized by the external-external-exchanged OPE coefficients.[11] Thus, the corresponding SDPs usually depend on two classes of parameters: the scaling dimensions of the external operators and the external-external-exchanged OPE coefficients for the isolated exchanged operators. In typical bootstrap studies one wants to map out the allowed region (i.e., the region consistent with the crossing equations) in the parameter space. For every point in the parameter space, `SDPB` can tell us if the point is allowed or not. We perform a scan of the parameter space by running `SDPB` for many points and then infer the shape of the boundary of the allowed region.[12]

[10] *Extraordinary* here refers to the enhanced boundary interactions needed to realize this transition, as opposed to the "ordinary" transition happening when boundary interactions have the same strength as the bulk ones. This terminology is the same as in the Ising case: $N = 1$. For $N \ge 2$ the transition is referred to as extraordinary-log because of logarithmic corrections in correlation functions.

[11] While for nonisolated exchanged operators we have a positive-semidefinite matrix without rank restriction.

[12] Here we are describing the so-called oracle mode, which was the standard way to run bootstrap computations before the advent of the navigator function, which is described in Sec. VI.

As we consider correlators involving more and more external operators, the dimension of the parameter space increases rapidly. Exploring such a high dimensional space is a major challenge for numerical bootstrap study of large correlator systems. A brute force scanning approach would suffer from the "curse of dimensionality," as the number of SDP runs increases exponentially with the dimension of space. Here we highlight the algorithms developed by Chester *et al.* (2020, 2021), which partially address this challenge. Using those algorithms, the aforementioned researchers achieved significant progress on the critical exponents of 3D O(2) and O(3) vector models. We now review the main concepts and these applications.

A. Algorithms

As mentioned, we must perform a scan in the space of scaling dimensions times the OPE coefficients. These two scanning directions are handled separately. For the scaling dimensions one uses an adaptive sampling method called Delaunay triangulation to map out the boundary of the allowed region. One first computes a grid of points that contains both allowed and disallowed points, then one applies the Delaunay triangulation (Wikipedia, 2024a), which finds a special set of triangles that link those points. The triangles that contain both allowed and disallowed points are the triangles covering the boundary. The area of those triangles roughly indicates the local resolution of the boundary. One then ranks the triangles by area and samples the middle points of the largest triangles; i.e., one focused on improving the regions with low resolution. This method is essentially a higher-dimensional generalization of the 1D bisection method. It works well in 2D and 3D space. This was sufficient for the applications of Chester *et al.* (2020, 2021). For higher-dimensional space the computations become much slower and the curse of the dimensionality strikes back.

As for the scan in the space of the OPE coefficients, Chester *et al.* (2020) developed a novel method called the cutting-surface algorithm, which is significantly faster than the Delaunay triangulation method. Here we describe the basic idea using a low-dimensional example and then discuss the higher-dimensional case.

A nondegenerate isolated internal operator gives rise to a term in the crossing equation of the form $\lambda^T \cdot \vec{V} \cdot \lambda$, where $\lambda \in \mathbb{R}^n$ is the vector of its OPE coefficients with the external operators and $\vec{V}$ is a vector of $n \times n$ matrices. Given a trial point λ_1, we use SDPB to look for a functional α_1 such that $\lambda_1^T \cdot \alpha_1(\vec{V}) \cdot \lambda_1 \geq 0$. If such a functional exists, the point λ_1 is ruled out; otherwise, one concludes that λ_1 is an allowed point. The key observation is that α_1, if it exists, rules out not only λ_1 but also a sizable disallowed region around λ_1. If λ is a 2D vector, this disallowed region can easily be found by explicitly solving the quadratic inequality[13] $\lambda^T \cdot \alpha_1(V) \cdot \lambda \geq 0$. The next trial point λ_2 can now be chosen outside of this disallowed region, etc. The disallowed region, which is the union of disallowed regions of $\lambda_1, \lambda_2, \ldots$, quickly grows. In the end one ends up with an allowed point, or the disallowed region covers the entire space.

When $\lambda \in \mathbb{R}^n$, $n \geq 3$, the disallowed region has to be defined implicitly by a set of quadratic inequalities $\lambda^T \cdot \alpha_i(V) \cdot \lambda \geq 0$, $i = 1, \ldots, k$. One decides the new trial λ_{next} in step $k+1$ by two steps: (1) try to find a point that is outside the disallowed region, i.e., $\lambda_{\text{next}}^T \cdot \alpha_i(V) \cdot \lambda_{\text{next}} < 0$ for all α_i, and (2) try to move this point away from the disallowed region as much as possible. The reason for step (2) is that, if the new point λ_{next} is chosen roughly at the center of the undetermined region, the new functional α_{next} (if it exists) usually rules out half of that region. Since each iteration cuts off about half of the volume, the total number of steps to achieve the needed accuracy grows roughly linearly in n. This is a much faster performance than for the Delaunay triangulation, achievable thanks to the quadratic structure of the constraints. Step (1) is a type of problem called a quadratically constrained quadratic program (QCQP), which is NP hard in general. However, for the problem at hand, Chester *et al.* (2020) found several heuristic approaches that work. The heuristics are not rigorous and should not be expected to solve generic QCQPs. What sets our problem apart is that one often has some idea about the expected size of the OPE coefficients, and a bounding box can then be set to constrain the space. With a suitable bounding box, those heuristics work well, at least when the number of OPE coefficients is not too large. When the heuristics fail to find an allowed point, one declares that the OPE coefficient space is ruled out. To speed up the computation, each SDP computation is "hot started" (Go and Tachikawa, 2019); namely, one reuses the final state of the SDP solver from the previous computation as the initial state in the new computation.

To combine Delaunay triangulation with cutting surface, one proceeds as follows. To begin, one chooses a grid of points in the space of scaling dimensions and computes the allowedness of each point, which means using the cutting-surface algorithm to rule out (or find allowed) OPE coefficients inside the bounding box (at fixed scaling dimensions). Then one uses the Delaunay triangulation to refine the grid in the space of scaling dimensions. This combined algorithm is suitable for two or three scaling dimensions, and a few OPE coefficients.[14] It is implemented in both `hyperion` and `simpleboot` frameworks.

B. Application to the O(2) model: The ν controversy resolved

The 3D O(2) universality class describes critical phenomena in many physical systems and has been studied intensively both experimentally and theoretically. Experimentally the most precise measurement of the 3D O(2) critical exponents came from the study of the ^{4}He superfluid phase transition on the Space Shuttle *Columbia* in 1992 (Lipa *et al.*, 1996, 2000, 2003). The critical exponent ν obtained from the data analysis of this experiment was $\nu^{\text{exp}} = 0.6709(1)$.

[13] As the condition is invariant under rescalings, it is enough to consider $\lambda = (1, \bar{\lambda})$.

[14] Chester and Su (2022) used the algorithm to scan seven ratios of OPE coefficients. As the number of OPE coefficients grows, one generally has to set a smaller bounding box; otherwise, the heuristics for the QCQP might fail.

TABLE II. Results of Chester *et al.* (2020) for the scaling dimensions of s, ϕ, and t, the leading charge 0, 1, and 2 scalars. The uncertainties in boldface are rigorous.

CFT data	Value
Δ_s	1.51136(**22**)
Δ_ϕ	0.519 088(**22**)
Δ_t	1.236 29(**11**)

Theoretically the simplest description in continuum field theory is given by the Lagrangian, where the mass term m^2 needs to be fine-tuned to reach the critical point,

$$\mathcal{L} = \frac{1}{2}|\partial\vec{\phi}|^2 + \frac{1}{2}m^2|\vec{\phi}|^2 + \frac{g}{4!}|\vec{\phi}|^4, \tag{4}$$

where ϕ transforms in the fundamental representation of O(2) and $s = |\vec{\phi}|^2$ is the leading singlet. Their scaling dimensions are related to critical exponents by

$$\Delta_\phi = \frac{1+\eta}{2}, \qquad \Delta_s = 3 - \frac{1}{\nu}. \tag{5}$$

The scaling dimensions can be calculated using the renormalization group method. More accurate results, however, came from the Monte Carlo (MC) simulation of (Hasenbusch, 2019), which estimated $\nu^{\text{MC}} = 0.67169(7)$. There is a 8σ difference between ν^{MC} and ν^{exp}.

The bootstrap study of the 3D O(N) model was initiated by Kos, Poland, and Simmons-Duffin (2014b), who considered the correlation function $\langle\phi_i\phi_j\phi_k\phi_l\rangle$. Later Kos *et al.* (2015, 2016) bootstrapped all correlation functions of ϕ, s, which allowed them to constrain the scaling dimensions Δ_ϕ and Δ_s to an island, although the size of that island was not yet sufficiently small to discriminate between ν^{MC} and ν^{exp}.

Finally, Chester *et al.* (2020) considered an even larger system of correlation functions that involved three relevant fields of this model as external operators: scalars ϕ and s and the charge-2 operator $t_{ij} = \phi_i\phi_j - (1/2)\delta_{ij}(\phi_k\phi^k)$. Since they employed the cutting-surface algorithm and pushed the computation to a high derivative order, Chester *et al.* were able to resolve the $\nu^{\text{MC}}/\nu^{\text{exp}}$ puzzle, as we now describe.[15] The assumptions of Chester *et al.* (2020) on the spectrum are that ϕ, s, and t are the only relevant operators in the charge-0, charge-1, and charge-2 sectors, with the charge-3 scalars[16] having a dimension larger than 1 and all charge-4 scalars irrelevant.[17] These assumptions are physically reasonable.

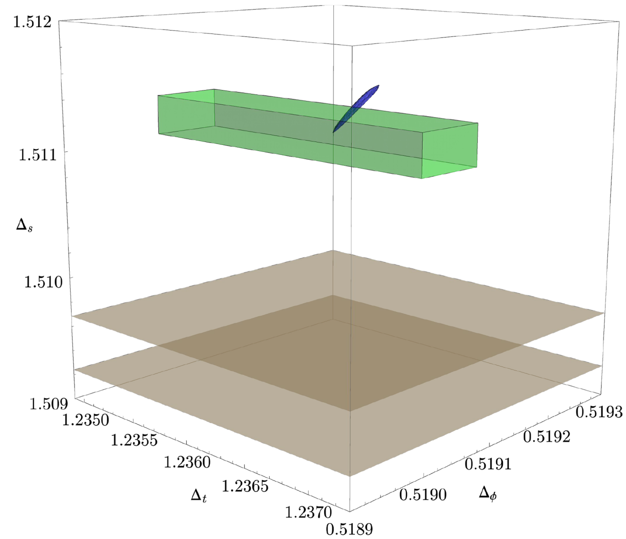

FIG. 4. The blue (dark gray) island is the allowed region from Chester *et al.* (2020) for the scaling dimensions of s, ϕ, and t. The green (gray) box indicates results from the Monte Carlo studies (Hasenbusch and Vicari, 2011; Hasenbusch, 2019). The brown (gray) planes represent the 1σ confidence interval from the experiment (Lipa *et al.*, 2003). From Chester *et al.*, 2020.

Under these assumptions, Chester *et al.* (2020) explored the parameter space spanned by three dimensions of $\{\phi, s, t\}$ and three OPE coefficient ratios $\{\lambda_{sss}/\lambda_{\phi\phi t}, \lambda_{\phi\phi s}/\lambda_{\phi\phi t}, \lambda_{tts}/\lambda_{\phi\phi t}\}$. The previously described Delaunay triangulation combined with the cutting-surface algorithm was used to scan over this six-dimensional space efficiently. The most constraining computation was done at the derivative order $\Lambda = 43$ and consumed 1.03 million CPU core hours. The results are summarized in Table II and Fig. 4.

The determined Δ_s translates into the critical exponent ν from the conformal bootstrap: $\nu^{\text{CB}} = 0.671\,754(\mathbf{99})$. The uncertainty in boldface is rigorous because it was determined from an allowed bootstrap island, which may only shrink as more and more constraints are added in future studies.[18] This value is consistent with ν^{MC} but decisively rules out the experimental measurement ν^{exp}. It would be interesting to perform a new statistical analysis of the experimental data to

[15]The analysis with three external operators was also carried out by Go and Tachikawa (2019). Without the cutting-surface algorithm, they could go only to a relatively low derivative order that was not sufficient to solve the puzzle.

[16]The leading charge-3 scalar dimension is ≈2.1.

[17]In addition, minuscule gaps above the unitarity bound were assumed in many sectors. This is reasonable since we do not expect any operators at unitarity other than the stress tensor and the conserved current. The technical reason for this assumption is to avoid poles of the conformal blocks at the unitarity bound, which interfere with the SDP numerics. See Chester *et al.* (2020) for an explanation.

[18]For completeness it should be mentioned that there are some other sources of "error in the error" that are not fully rigorous, although they are under control. For example, conformal block derivatives are replaced by their rational approximations when they are passed to an SDP. The error from this approximation is monitored, and we estimate its effect to be orders of magnitude smaller than the previously reported main error coming from the size of the bootstrap island. If needed, this error can easily be further decreased. Another nonrigorous error comes from the Delaunay triangulation method and the heuristics in the cutting-surface algorithm not being completely rigorous. Chester *et al.* (2020) took measures to control this issue. For example, the reported error bar has added uncertainty in the Delaunay triangulation method, which is roughly represented by the size of the triangle on the boundary. These sources of error could be completely removed by repeating the study of Chester *et al.* (2020) using the navigator method of Sec. VI.

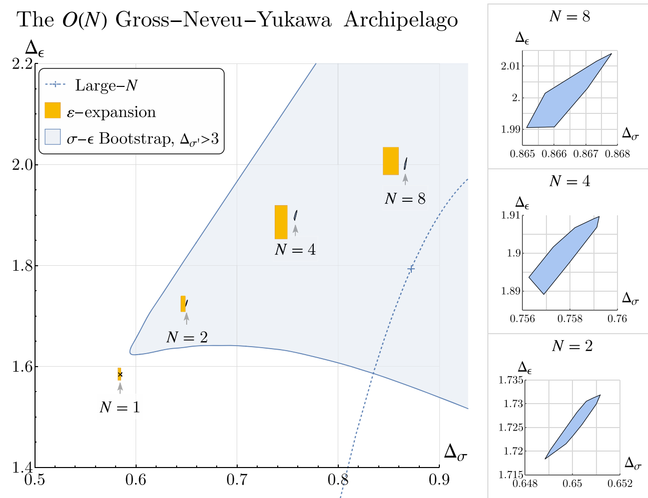

FIG. 5. Right panels: enlarged bootstrap islands for the $N = 2, 4$, and 8 O(N) GNY model from Erramilli *et al.* (2023) at $\Lambda = 35$ projected onto the $(\Delta_\sigma, \Delta_\epsilon)$ plane. Left panel: enlarged view of the same islands. Dotted blue curve: perturbative estimates in the large-N expansion. Orange (dark gray) boxes: Borel resummations of the $4 - \epsilon$ expansion (Ihrig, Mihaila, and Scherer, 2018). The **x** indicates the location of the $N = 1$ island of Atanasov *et al.* (2022). Light blue (light gray) region: the general $\sigma - \varepsilon$ bootstrap bounds with the assumption $(\Delta_{\sigma'} > 3)$ from Atanasov, Hillman, and Poland (2018). Bootstrap islands do not overlap with the orange (dark gray) boxes for $N = 2$, 4, and 8, implying that the error bar of the Borel-resummed results was underestimated. Adapted from Erramilli *et al.* 2023.

understand whether the experimental error was perhaps underestimated.

C. Application to the O(N) Gross-Neveu-Yukawa model

The Gross-Neveu-Yukawa (GNY) model with O(N) symmetry is described by the following Lagrangian:

$$\mathcal{L} = \frac{1}{2}(\partial\phi)^2 + \frac{i}{2}\psi_i \partial\!\!\!/ \psi_i + \frac{1}{2}m^2\phi^2 + \frac{\lambda}{2}\phi^4 + i\frac{g}{2}\phi\psi_i\psi_i, \qquad (6)$$

where ϕ is a parity-odd scalar and ψ represents N Majorana fermions transforming in the vector representation of O(N). The O(N) singlet ϕ couples to ψ_i through the Yukawa coupling term $\phi\psi_i\psi_i$. At a certain value of the mass m, the model becomes critical and flows to a CFT. When $N = 1$, the model is the same as Eq. (1) and is expected to exhibit emergent $\mathcal{N} = 1$ supersymmetry.

The large-N expansion of the scaling dimensions of various operators in this model was computed by Gracey (2018) and Manashov and Strohmaier (2018). Based on the large-N results, some important features of the spectrum are (1) there is only one single relevant operator: $\epsilon \sim \phi^2$; (2) owing to the equation of motion, the leading parity-even fermion $\chi_i \sim \phi^3\psi_i$ has a large scaling dimension, and large-N expansion predicts $\Delta_\chi \geq 4$; and (3) although not obvious from the equation of motion, in large-N computations, $\sigma \sim \phi$ is the only relevant parity-odd singlet for $N \geq 2$.

These features are suitable as input for a bootstrap study of the CFT. Erramilli *et al.* (2023) conducted a bootstrap analysis on all four-point functions of σ, ϵ, and ψ_i with reasonable and mild assumptions on $\Delta_{\sigma'}, \Delta_{\epsilon'}, \Delta_{\psi'}$, and $\Delta_{\chi'}$, where $\mathcal{O}'$ denotes the next operator in the same sector as $\mathcal{O}$. The conformal block decomposition involving fermions was effectively computed using `blocks_3d`; see Sec. II.A.

To impose the condition that σ, ϵ, and ψ are the only operators at their scaling dimensions, one must scan over the OPE coefficients involving only external operators. Therefore, the free parameters include the scaling dimensions Δ_σ, Δ_ϵ, and Δ_ψ and the OPE coefficients $\lambda_{\psi\psi\sigma}, \lambda_{\psi\psi\epsilon}, \lambda_{\sigma\sigma\epsilon}$, and $\lambda_{\epsilon\epsilon\epsilon}$. Like Chester *et al.* (2020), Erramilli *et al.* (2023) applied the Delaunay search algorithm to scan over the scaling dimensions, and the cutting-surface algorithm to scan over the three ratios of OPE coefficients. These techniques sufficed to obtain interesting results, which we now describe.

For $N = 1$, Erramilli *et al.* (2023) assumed $\Delta_{\sigma'} > 2.5$, $\Delta_{\epsilon'} > 3$, $\Delta_{\psi'} > 2$, and $\Delta_{\chi'} > 3.5$ and found an isolated region. The super-Ising island of Atanasov *et al.* (2022) is located at the tip of this isolated region. Without assuming supersymmetry, Erramilli *et al.* (2023) determined whether a conserved supercurrent exists in the isolated region. Near the tip corresponding to the range of parameters in Table I, the spin-3/2 upper bound was found to be $\Delta_{\rm SC} < 2.500\,321\,9$, which is close to the exactly conserved supercurrent dimension 2.5. This implies that any CFT with these parameters must be, to an extremely high degree of precision, supersymmetric, which is strong evidence for the emergent supersymmetry scenario.

For $N = 2$, 4, and 8, Erramilli *et al.* (2023) assumed that $\Delta_{\sigma'} > 3, \Delta_{\epsilon'} > 3, \Delta_{\psi'} > 2$, and $\Delta_{\chi'} > 3.5$ and found small bootstrap islands for those theories. Figure 5 shows these islands at $\Lambda = 35$, and the scaling dimensions with rigorous error bars are summarized in Table III.

Note that there is another closely related Lagrangian

$$\mathcal{L} = \frac{1}{2}(\partial\phi)^2 + \frac{i}{2}\psi_i^A \partial\!\!\!/ \psi_i^A + \frac{1}{2}m^2\phi^2 + \frac{\lambda}{2}\phi^4 + i\frac{g_1}{2}\phi(\psi_i^L\psi_i^L - \psi_i^R\psi_i^R) + i\frac{g_2}{2}\phi(\psi_i^L\psi_i^L + \psi_i^R\psi_i^R), \qquad (7)$$

TABLE III. Scaling dimensions and critical exponents obtained in for the O(N) GNY model, with rigorous error bars indicated in boldface (Erramilli *et al.*, 2023).

	Δ_ψ	Δ_σ	Δ_ϵ	η_ψ	η_ϕ	ν^{-1}
$N = 2$	1.068 61(**12**)	0.6500(**12**)	1.725(**7**)	0.137 22(**24**)	0.3000(**23**)	1.275(**7**)
$N = 4$	1.043 56(**16**)	0.7578(**15**)	1.899(**10**)	0.08712(**32**)	0.5155(**30**)	1.101(**10**)
$N = 8$	1.021 19(**5**)	0.8665(**13**)	2.002(**12**)	0.042 38(**11**)	0.7329(**27**)	0.998(**12**)

where $i = 1, \ldots, N/2$ is an $\mathrm{O}(N/2)$ vector index and $A = L$ and R labels two species of fermions. If $g_1 = 0$ and $g_2 \neq 0$, this corresponds to the $\mathrm{O}(N)$ GNY Lagrangian (6), and its fixed point was bootstrapped by Erramilli *et al.* (2023). If $g_1 \neq 0$ and $g_2 = 0$, the model has $\mathrm{O}(N/2)^2 \rtimes Z_2$ symmetry, where Z_2 is realized by $\psi_i^L \leftrightarrow \psi_i^R$ and $\phi \to -\phi$. At a critical value of mass, the $\mathrm{O}(N/2)^2 \rtimes Z_2$ GNY model is expected to flow to the "chiral Ising" universality class, which is different from the $\mathrm{O}(N)$ GNY CFT. Various Monte Carlo simulations (Huffman and Chandrasekharan, 2020; Liu, Wang *et al.*, 2020) have been used to study this phase transition.[19] There are interesting applications of this model in graphene and D-wave superconductors; see Erramilli *et al.* (2023) for a summary. It would be interesting to see if future bootstrap studies of the $\mathrm{O}(N/2)^2 \rtimes Z_2$ GNY CFT can distinguish its critical exponents from those of the $\mathrm{O}(N)$ GNY CFT.

V. `tiptop`

In many situations we are interested in the maximum or minimum value of a certain parameter over the allowed region. The `tiptop` algorithm (Chester *et al.*, 2021) was designed to explore the "tip" of a convex region. Like Delaunay triangulation, `tiptop` usually works in pairs with the cutting-surface algorithm: `tiptop` recommends new points near the tip in a direction of a certain scaling dimension, while the cutting-surface algorithm is called to decide the (dis)allowedness of those points. In this section we describe this algorithm and its application to the 3D $\mathrm{O}(3)$ vector model. The algorithm was also used by Mitchell and Poland (2024) to bound the leading irrelevant operator of the 3D Gross-Neveu-Yukawa CFTs from Sec. IV.C.

A. The `tiptop` algorithm

We consider a bootstrap problem depending on $n+1$ parameters: $x \in \mathbb{R}^n$ and y. We want to know the maximum value of y in the allowed region. For example, x may comprise n scaling dimensions and y, another scaling dimension that we are particularly interested in. We assume that the allowed region around the maximum y is convex, so as y increases the allowed region of x (for a fixed y) shrinks to zero size. The `tiptop` algorithm starts with some disallowed points and at least one allowed point at current $y = y_{\text{allowed}}$. Given a list of allowed, disallowed, and in-progress points (which are treated as disallowed by `tiptop`), the algorithm recommends one point to look at next.

To do that, `tiptop` first verifies that the shape and the size of the allowed region at y_{allowed} are well understood. An affine coordinate transformation of the x space is performed such that the region of known allowed x at y_{allowed} is roughly spherical.[20] The full region of interest is then rescaled so that it is the cube $[-1, 1]^n$. One recursively subdivides this region into *cells*, which are cubes of size 2^{-k}, $k = 0, 1, \ldots, \min(K, k_{\max})$, where K is the first integer such that 2^{-K} is less than f times the minimum coordinate extents of the set of allowed points, f is a user-defined parameter (for example, $f = 2$ works well), and[21] $k_{\max} = 47$. The algorithm then recommends a new point to be placed in the largest empty cell (i.e., a cell in which there is no point), which is diagonally adjacent to a cell containing allowed points.

If there is no such empty cell, the shape of the allowed region at y_{allowed} is considered well understood. In this case the algorithm recommends a new point at a higher y. The x of the new point is roughly at the center of the allowed points at y_{allowed}, while y is halfway between y_{allowed} and y_{ceiling} (i.e., a bisection step). At first, y_{ceiling} is a user-defined value that is safely larger than $y_{\max}$. After some points have been checked, y_{ceiling} is the lowest disallowed y. If $y_{\text{allowed}} - y_{\text{ceiling}}$ is smaller than a certain user-specified value, the algorithm stops.

B. Application to the $\mathrm{O}(3)$ instability problem

The $\mathrm{O}(3)$ vector model can be defined by the Lagrangian (4) with ϕ in the vector representation of $\mathrm{O}(3)$. Alternatively, the Heisenberg model on the cubic lattice with the Hamiltonian

$$\mathcal{H} = -J \sum_{\langle x,y \rangle} \sigma_x \cdot \sigma_y, \tag{8}$$

where $\sigma_x \in \mathbb{R}^3$ are classical spins of unit length, has the phase transition in the same universality class.

Chester *et al.* (2021) bootstrapped correlators of ϕ, s, and t, which are the leading scalars in the $\mathrm{O}(3)$ vector, singlet, and rank-2 traceless symmetric tensor irreducible representations (irreps). The bootstrap setup of the $\mathrm{O}(3)$ CFT is similar to the $\mathrm{O}(2)$ case, except that there are more irreducible representation channels in the OPE expansion $t \times t$. Of particular interest is the operator t_4, the leading four-index traceless symmetric tensor appearing in this OPE.

With the assumption that ϕ, s, and t are the only relevant scalars in their representation, Chester *et al.* (2021) made two bootstrap computations. In the first computation a conservative assumption $\Delta_{t_4} \geq 2$ was made. Then Delaunay triangulation and cutting surface were used to map out the $\mathrm{O}(3)$ allowed island at the derivative order $\Lambda = 43$. Rigorous results for the scaling dimensions of s, ϕ, and t from this computation are given in Table IV.

In the second computation Chester *et al.* (2021) used the `tiptop` algorithm to find a rigorous upper bound on Δ_{t_4}, with the result $\Delta_{t_4} \leq 2.990\,56$ at $\Lambda = 35$. Therefore, t_4 is relevant, although weakly so. Figure 6 indicates the progress of `tiptop` as it maximizes Δ_{t_4}.

The relevance of t_4 is important for the structure of the RG flow. Since t_4 is relevant, the Heisenberg fixed point is unstable with respect to perturbations by a linear combination of components of t_4. A particularly interesting linear combination is

$$\sum_{i=1}^{3} (t_4)_{iiii}, \tag{9}$$

[19] We thank Yin-Chen He for clarifying this point.

[20] The affine transformation is needed because isolated allowed regions in conformal bootstrap tend to have extreme aspect ratios.

[21] The value of $k_{\max}$ was chosen so that $2^{-k_{\max}}$ is somewhat larger than the minimum resolution of an IEEE-754 double-precision number.

TABLE IV. Conformal bootstrap results of Chester *et al.* (2021) for the scaling dimensions of s, ϕ, and t, the leading scalars in the O(3) vector, singlet, and rank-2 traceless symmetric tensor irreps. The boldface uncertainties are rigorous.

CFT data	Value
Δ_s	$1.594\,88(\mathbf{81})$
Δ_ϕ	$1.518\,936(\mathbf{61})$
Δ_t	$1.209\,54(\mathbf{32})$

which preserves the symmetry group $B_3 \equiv S_3 \ltimes (\mathbb{Z}_2)^3 \subset \mathrm{O}(3)$, which is called the cubic group.[22] This triggers an RG flow to another fixed point called the cubic fixed point (Aharony, 1973), whose symmetry group is B_3. Since t_4 is so weakly relevant, this RG flow is extremely short, and the critical exponents of the Heisenberg and cubic fixed point are close to each other.

Previously the relevance of t_4 was studied for many decades in perturbation theory. These studies compute the critical exponent $Y = 3 - \Delta_{t_4}$. Since Y is close to zero, it is not easy to determine its sign. By 2000, RG studies had agreed upon the conclusion that $Y_{\mathrm{O}(3)} > 0$ at the Heisenberg fixed point, while $Y_{B_3} < 0$ at the cubic fixed point; see Pelissetto and Vicari (2002). However, the error bars of these studies were significant, and the sign of Y was determined only at a 2σ level. Monte Carlo simulations improved this to 3σ in 2011 (Hasenbusch and Vicari, 2011). The aforementioned bootstrap result gives a rigorous proof showing that t_4 is indeed relevant.[23]

We now discuss phenomenological implications of the relevance of t_4. For ferromagnets this is not so important: the perturbing cubic coupling (9) will have for them a small coefficient having spin-orbit origin. An example of when this term is important is the structural phase transition in perovskites. Perovskites like $SrTiO_3$ and $LaAlO_3$ have crystal cells preserving cubic symmetry at high temperature. As temperature decreases below a certain critical temperature T_c, the materials undergo a structural phase transition, where the lattice is stretched in a direction along an axis or a diagonal. Using the Landau theory, one can model this phase transition via the potential $\mu|\vec{\phi}|^2 + u|\vec{\phi}|^4 + v\sum_{i=1}^{3}(\phi_i)^4$, where $v > 0$ and $v < 0$ correspond to the order parameter ϕ breaking the cubic symmetry along an axis or a diagonal.[24] RG studies show that the (stable, as we now know for sure) cubic fixed point lies at $v > 0$. The RG flow diagram is as in Fig. 7. It follows that perovskites like $SrTiO_3$ whose low-T structure breaks the cubic symmetry along an axis will have a first-order phase transition, while $LaAlO_3$, whose structure breaks cubic symmetry along a diagonal, will have a second-order phase transition in the cubic universality class (Aharony, Entin-Wohlman, and Kudlis, 2022). However, since Y is so small, the flow is attracted to the cubic fixed point slowly along the v direction. Hence, we expect strong corrections to scaling.

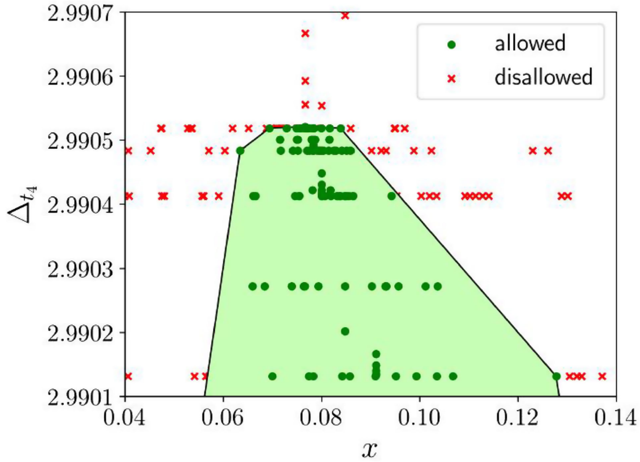

FIG. 6. Two-dimensional projection of the progress of `tiptop` as it maximizes Δ_{t_4}. From Chester *et al.*, 2021.

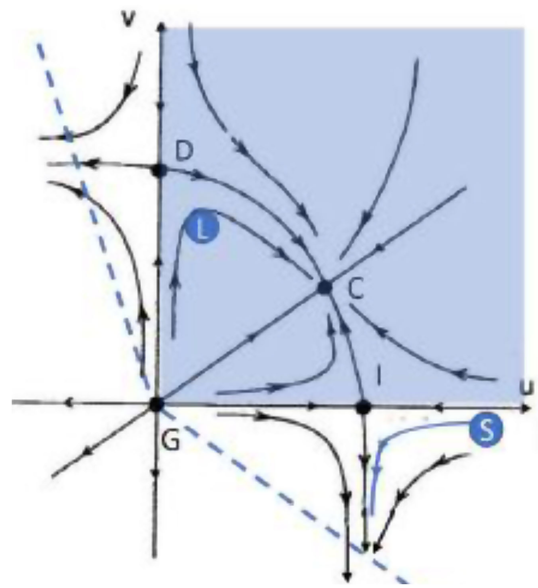

FIG. 7. RG flow in the coupling plane (u, v) for the case t_4 is irrelevant at the Heisenberg fixed point (I), driving the flow to the cubic fixed point (C), located at $v > 0$. The distance between C and I is exaggerated: in reality these fixed points are close to each other. Also shown in this diagram is the schematic position of $SrTiO_3$ (S) flowing to a first-order transition and $LaAlO_3$ (L), which is attracted to the cubic fixed point and should show a second-order transition with significant corrections to scaling. From Aharony, Entin-Wohlman, and Kudlis, 2022.

VI. NAVIGATOR FUNCTION

A. General idea

Delaunay triangulation, surface cutting, and `tiptop` algorithms from the previous sections alleviate the curse of

[22] S_3 permutes the three coordinate axes, and the $(\mathbb{Z}_2)^3$ flips those three axes.

[23] Hasenbusch (2023) has since obtained an accurate Monte Carlo determination $Y_{\mathrm{O}(3)} = 0.0142(6)$ and $Y_{B_3} = -0.0133(8)$, while a conformal bootstrap calculation with v, s, t_2, and t_4 external scalars (Rong and Su, 2023) computed the OPE coefficients of the t_4 operator and set up a conformal perturbation theory computation predicting the cubic theory exponents in terms of the O(3) ones.

[24] Plotting the potential with $\mu < 0$ and $v > 0$, one can see that the minimum of the potential is along the diagonals, and with $\mu < 0$ and $v < 0$ the minimum is along the axes.

dimensionality in determining the shape of the allowed region. All of these algorithms use SDPB in the oracle mode while testing individual points for being allowed or disallowed. The navigator function method (Su, 2020; Reehorst *et al.*, 2021) is a radically new idea that departs from the oracle philosophy. In this method a single SDPB run returns not the 0 (1) information for allowed (disallowed), but instead a real number whose sign indicates whether it is allowed or disallowed, while the magnitude shows how far the tested point is from the allowed region boundary. This leads to even more efficient strategies for multiparameter bootstrap studies.

As usual, we consider a bootstrap problem characterized by a finite vector of parameters x. Typically x includes scaling dimensions of a few operators, their OPE coefficients, and spectrum gap assumptions. Spacetime dimension d and the global symmetry group parameters [such as N for the $O(N)$ symmetry] may also be included in x.

The navigator function (Reehorst *et al.*, 2021) is a continuous differentiable function $\mathcal{N}(x)$ whose sublevel set $\{x : \mathcal{N}(x) \le 0\}$ coincides with the allowed region A. This function is generally not convex. However, in many examples that have been considered, the function was found to have a convex shape in the neighborhood of an isolated allowed region (see the Appendix), with a single minimum inside it; see Fig. 8. This property translates into the fact that isolated allowed regions in the conformal bootstrap often have elliptical shapes that shrink with the increase of the derivative order Λ. We later see how to set up such a navigator function and compute it using SDPB. The gradient $\boldsymbol{\nabla}\mathcal{N}(x)$ is also inexpensive to compute (Reehorst *et al.*, 2021). This is because the navigator is given as a result of an optimization problem, and first-order variations of the objective at extremality can be found without computing the change in the minimizer.[25]

A typical task from which any bootstrap study starts is to find a single allowed point. This may be nontrivial if one works at a high derivative order so that the allowed region is small. With the navigator function an allowed point is searched for by minimizing $\mathcal{N}(x)$ via a quasi-Newton method (Reehorst *et al.*, 2021) such as the Broyden-Fletcher-Goldfarb-Shanno (BFGS) algorithm (Wikipedia, 2024b). We start with an initial guess x_0 in the excluded region and proceed through a sequence of points $x_0 \to x_1 \to x_2 \to \cdots$. If the allowed region is not empty, we will reach it after a finite number of steps. If, on the contrary, we reach a positive minimum of $\mathcal{N}(x)$, we conclude that the allowed region is empty.

Another typical task is to understand the shape of the allowed region. The boundary is the zero set of the navigator $\{x : \mathcal{N}(x) = 0\}$. In the case of a 2D allowed region, when the boundary is a curve, we can fully trace it out by making small steps tangential to the boundary and then projecting back to the boundary while taking advantage of the available $\boldsymbol{\nabla}\mathcal{N}(x)$. For a higher-dimensional allowed region, we can try to understand the shape of the boundary by understanding its 1D curvilinear sections through various hyperplanes.

[25]This is true even for constrained minimization, as in our case, when a primal-dual optimization method such as SDPB is used.

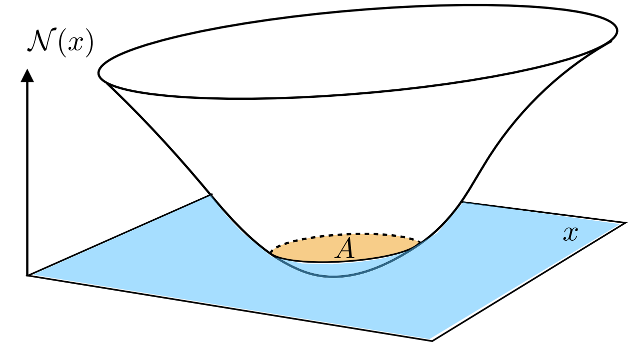

FIG. 8. Schematic of the navigator function $\mathcal{N}(x)$. The allowed region $A = \{x : \mathcal{N}(x) \le 0\}$.

However, this may be expensive. On the positive side, we are often interested in extremal allowed values in certain directions rather than in the precise shape of the allowed region. We can move inside the allowed region until we hit an extremal point on the boundary in a certain direction, as was done by Reehorst *et al.* (2021, 2024). This strategy supersedes the tiptop algorithm.

B. Existence and gradient

It is not trivial that the navigator function exists. We explain why this is so using the prototypical example of a single-correlator crossing equation

$$\sum_{\mathcal{O} \in \phi \times \phi} p_{\phi\phi\mathcal{O}} F_{\Delta,\ell}(u,v) = 0, \qquad p_{\phi\phi\mathcal{O}} \ge 0. \tag{10}$$

We impose the constraints that

$$\ell = 0:\ \Delta = 0\,(\text{unit operator}) \quad \text{or} \quad \Delta \ge \Delta_*, \tag{11}$$

while for $\ell > 0$ all Δ must be at or above the unitarity bound Δ_ℓ. Equation (10) with these constraints is the primal problem, depending on $x = (\Delta_\phi, \Delta_*)$. The dual problem is obtained by considering a linear functional α such that

$$\begin{aligned} &\alpha[F_{\Delta=0,\ell=0}(u,v)] > 0, \\ &\alpha[F_{\Delta,\ell=0}(u,v)] \ge 0 \quad \text{for } \Delta \ge \Delta_*, \\ &\alpha[F_{\Delta,\ell}(u,v)] \ge 0 \quad \text{for } \Delta \ge \Delta_\ell. \end{aligned} \tag{12}$$

As usual, if α solving the dual problem exists, then there is no $p_{\phi\phi\mathcal{O}} \ge 0$ solving the primal problem and x is disallowed.

The navigator function is defined by solving the following modified dual problem with an objective,

$$\begin{aligned} &\mathcal{N}(x) = \max_\alpha \alpha[F_{\Delta=0,\ell=0}(u,v)], \quad \text{where} \\ &\alpha[F_{\Delta,\ell=0}(u,v)] \ge 0 \quad \text{for } \Delta \ge \Delta_*, \\ &\alpha[F_{\Delta,\ell}(u,v)] \ge 0 \quad \text{for } \Delta \ge \Delta_\ell, \\ &\alpha[F_{\text{norm}}(u,v)] = 1. \end{aligned} \tag{13}$$

This problem is of a form that can be handled with SDPB. The normalization vector $F_{\text{norm}}(u,v)$ should be chosen appropriately to ensure that the navigator is finite. The criterion for this choice is that the $F_{\mathrm{norm}}(u,v)$ should lie strictly inside the cone $\mathcal{C}$, which is generated by all vectors $F_{\Delta,\ell}(u,v)$ that are allowed to appear in the crossing equation (Su, 2023). This leads to the first navigator construction of Reehorst *et al.* (2021), the Σ-navigator, when one chooses

$$F_{\mathrm{norm}}(u,v)=\sum_i F_{\Delta_i,\ell_i}(u,v) \tag{14}$$

for a finite set of Δ_i,ℓ_i satisfying the spectrum constraints.

In the primal formulation, one computes the navigator as

$$\mathcal{N}(x)=\min\lambda, \quad \text{where}$$
$$\sum_{\mathcal{O}\in\phi\times\phi} p_{\phi\phi\mathcal{O}}F_{\Delta,\ell}(u,v)-\lambda F_{\mathrm{norm}}(u,v)=0, \quad p_{\phi\phi\mathcal{O}}\geq 0. \tag{15}$$

Equation (15) leads to the second navigator construction of Reehorst *et al.* (2021), the GFF-navigator when one chooses $-F_{\mathrm{norm}}(u,v)$ to be the sum of a few conformal blocks of a generalized free field (GFF) solution to crossing. The GFF-navigator is bounded from above by 1.

C. Applications

Although recent, the navigator function method has already been applied in several studies that would be difficult or impossible to complete with previous techniques (Chester and Su, 2022; Reehorst, 2022; Sirois, 2022; Henriksson, Kousvos, and Reehorst, 2023). We now provide a description of these results.

1. Rigorous bounds on irrelevant operators of the 3D Ising CFT

Reehorst (2022) studied the 3D Ising model CFT using the navigator function that depends on 13 parameters: dimensions of five operators σ, ϵ, σ', ϵ', and T' (which is the first spin-2 operator after the stress tensor), the central charge c_T, and seven OPE coefficients $\lambda_{\sigma\sigma\varepsilon}$, $\lambda_{\varepsilon\varepsilon\varepsilon}$, $\lambda_{\sigma\sigma\varepsilon'}$, $\lambda_{\varepsilon\varepsilon\varepsilon'}$, $\lambda_{\sigma\varepsilon\sigma'}$, $\lambda_{\sigma\sigma T'}$, and $\lambda_{\varepsilon\varepsilon T'}$. Imposing the gaps $\Delta_{\sigma''}$, $\Delta_{\varepsilon''}$ and $\Delta_{T''}\geq 6$, he determined an allowed region for the navigator function parameters. This led to rigorous two-sided bounds on all of these parameters (Reehorst, 2022), for example,

$$\Delta_{\varepsilon'}=3.829\,51(\mathbf{61}) \quad (\Lambda=31). \tag{16}$$

Previously only four of these parameters, namely, Δ_σ, Δ_ε, $\lambda_{\sigma\sigma\varepsilon}$, and $\lambda_{\varepsilon\varepsilon\varepsilon}$ (Kos *et al.*, 2016), had such rigorous bounds. The bounds on other quantities were determined nonrigorously (Simmons-Duffin, 2017) by performing a partial scan over 20 points in the allowed island in the Δ_σ, Δ_ε, and $\lambda_{\sigma\sigma\varepsilon}/\lambda_{\varepsilon\varepsilon\varepsilon}$ space, minimizing c_T for each of them, extracting the spectrum via the extremal functional method (El-Showk and Paulos, 2013), and estimating errors as 1 standard deviation. For ε' this nonrigorous determination gave

$$\Delta_{\varepsilon'}=3.829\,68(23) \qquad (\Lambda=43). \tag{17}$$

where $\Lambda=43$ (Simmons-Duffin, 2017). We see that the rigorous determination (16), though consistent, has a larger error because it uses smaller Λ and because the nonrigorous method is based on a partial scan, which may further underestimate the error. Surprisingly, though, for some quantities the rigorous error turns out to be somewhat smaller than the nonrigorous one, despite smaller Λ, for example,

$$\lambda_{\varepsilon\varepsilon\varepsilon'}=\begin{cases}1.5362(\mathbf{12}) & (\Lambda=19),\\ 1.5360(16) & (\Lambda=43),\end{cases} \tag{18}$$

with quantities taken from Reehorst (2022) and Simmons-Duffin (2017), respectively. As explained by Reehorst (2022), in this case the nonrigorous $\lambda_{\varepsilon\varepsilon\varepsilon'}$ determination is polluted by outlier solutions that contain not one but two nearly degenerate operators near $\Delta_{\varepsilon'}$ sharing the OPE coefficient $\lambda_{\varepsilon\varepsilon\varepsilon'}$ [the sharing effect (Liu, Meltzer *et al.*, 2020)]. In the navigator function method of Reehorst (2022), the operator ε' is isolated by definition, excluding the sharing effect and leading to a more robust determination of $\lambda_{\varepsilon\varepsilon\varepsilon'}$.

2. Navigating through the O(N) archipelago

Previously Kos *et al.* (2015) studied the O(N) model in $d=3$ for discrete integer values of $N=1, 2, 3, \ldots$, using the scan method. Using the three-correlator setup $\langle\phi\phi\phi\phi\rangle$, $\langle\phi\phi ss\rangle$, and $\langle ssss\rangle$, where ϕ and s are the lowest scalars in the O(N) vector and singlet irreps, they isolated the O(N) model in $d=3$ to islands, which is referred to as the O(N) archipelago.

Recently, Sirois (2022) applied the navigator method to the O(N) model in the same three-correlator setup but made N and d vary continuously. The navigator function depended on the four arguments Δ_ϕ, Δ_s, $\lambda_{sss}/\lambda_{\phi\phi s}$, and Δ_t, where t is the lowest scalar in the O(N) symmetric traceless tensor irrep. A gap up to $\Delta=d$ was imposed in these three channels, as well as gaps of 0.5 above the stress tensor and the conserved current operators. With these assumptions, at $\Lambda=19$ Sirois (2022) followed the islands along three continuous families in the (d,N) space,[26]

$$\begin{aligned}&\{1\leq N\leq 3,\ d=3\},\\ &\{N=2\,,3\leq d\leq 4\},\\ &\{N=3,\ 3\leq d\leq 4\}.\end{aligned} \tag{19}$$

The position and size of the islands were determined along each line and compared to the predictions from the ϵ expansion, with good agreement found.

The work of Sirois (2022) adds further evidence that one should not be afraid to apply the unitary numerical conformal bootstrap method to models with noninteger N and d [for prior evidence in noninteger d, see El-Showk *et al.* (2014a), Cappelli, Maffi, and Okuda (2019), and Bonanno *et al.* (2023)]. Indeed, while such models are nominally nonunitary (Maldacena and Zhiboedov, 2013; Hogervorst, Rychkov, and Rees, 2015, 2016), unitarity violations are secluded at high operator dimensions and are invisible at the currently

[26]For the first family the navigator function depended on only three arguments Δ_ϕ, Δ_s, and Δ_t.

attainable numerical accuracy. This should be true as long as N and d are sufficiently large.

The situation changes, however, when N becomes too small.[27] For example, the limit $N \to 1$ is dangerous because the symmetric traceless and antisymmetric irreps used in the $\mathrm{O}(N)$ model bootstrap analysis do not exist for $N = 1$ (their dimension goes to zero as $N \to 1$). Sirois (2022) found that the island shrunk to zero size when $N \to 1^+$ as $d = 3$ [the first family in Eq. (19)]. This is because there are primary operators in the spectrum at $N > 1$ whose squared OPE coefficients go linearly to zero as $N \to 1^+$, thus preventing continuation of the unitary solution to crossing to $N < 1$. Numerically Sirois (2022) identified two such operators in the solution to crossing at $d = 3$. Analytically, similar phenomena were shown to occur in the free $\mathrm{O}(N)$ theory, and in the perturbative setting of $d = 4 - \epsilon$.

[27]And also when d is too small (Golden and Paulos, 2015).

3. Ising CFT as a function of d: Spectrum continuity and level repulsion

Previously the Ising CFT was studied as a function of $d \in [2, 4]$ using the single-correlator setup $\langle\sigma\sigma\sigma\sigma\rangle$, with the position of the theory identified with the kink in Δ_ε maximization (El-Showk *et al.*, 2014a) or in the c_T minimization (Cappelli, Maffi, and Okuda, 2019; Bonanno *et al.*, 2023). For the intermediate values $d = 3.25$, 3.5, the 3.75, islands were found via scans in the three-correlator setup $\langle\sigma\sigma\sigma\sigma\rangle$, $\langle\sigma\sigma\varepsilon\varepsilon\rangle$, and $\langle\varepsilon\varepsilon\varepsilon\varepsilon\rangle$ (Behan, 2017). All of these studies gave results that were in good agreement with the ϵ expansion.

Recently, Henriksson, Kousvos, and Reehorst (2023) carried out a systematic study of the Ising CFT spectrum for $2.6 \le d \le 4$ using the navigator function $\mathcal{N}(\Delta_\sigma, \Delta_\varepsilon, \lambda_{\varepsilon\varepsilon\varepsilon}/\lambda_{\sigma\sigma\varepsilon})$. Working at $\Lambda = 30$, the low-lying spectrum was extracted applying the extremal function method at the navigator minimum for several dimensions in the $2.6 \le d \le 4$ range.

This study led to two lessons. First, it provided further evidence that the spectrum of the Ising CFT varies continuously with d. Second, their important finding was the observation of an avoided level crossing between two scalar $\mathbb{Z}_2$-even operators ε'' and ε''', which start in $d = 4 - \varepsilon$ with $\Delta'' = 6 + O(\varepsilon)$ and $\Delta''' = 8 - O(\varepsilon)$. As d is lowered, the lowest-order ε expansion predicts a crossing in $d \approx 3.3$. The perturbative ε expansion does not take nonperturbative mixing effects between operators with the same quantum numbers into account. Such effects are expected to lead to avoided level crossings (Korchemsky, 2016; Behan, 2018), although the precise mechanism of how this happens when d is deformed has not yet been clarified. Henriksson, Kousvos, and Reehorst (2023) provided evidence for this scenario, as they observed that Δ'' and Δ''' do get close to each other and then repel around $d \approx 2.78$ with a minimal difference $(\Delta''' - \Delta'')_{\min} \approx 0.136$; see Fig. 9.

In the future it would be interesting to repeat the study of Henriksson, Kousvos, and Reehorst (2023) at higher Λ to determine $(\Delta''' - \Delta'')_{\min}$ more precisely and gain evidence that their avoided level crossing is not a finite Λ artifact. It would also be interesting to develop a theoretical

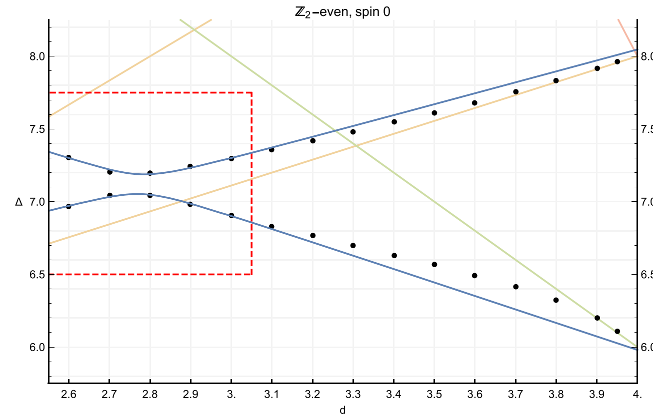

FIG. 9. Observation of the level repulsion effect. Black dots: spectrum from the bootstrap (extremal functional method). Blue (dark gray) curves: fitted hyperbola to the black dots within the dashed red box. Green (light gray) and orange (light gray) lines: predictions for operator dimensions from the lowest order $4 - \epsilon$ expansion. From Henriksson, Kousvos, and Reehorst, 2023.

understanding of the nonperturbative mixing effects that control $(\Delta''' - \Delta'')_{\min}$.

4. Three-state Potts model: Toward the upper critical dimension

The three-state Potts model has a second-order phase transition in $d = 2$, while it has a first-order phase transition in $d = 3$ (Janke and Villanova, 1997). It would be interesting to get a bootstrap proof of this fact, ruling out the existence of S_3 symmetric 3D CFTs that could describe such a transition (Rychkov, 2020). One would expect the critical and tricritical three-state Potts CFTs to merge and annihilate at some $d_c < 3$. Determining d_c would also be worthwhile.[28]

Recently, Chester and Su (2022) approached the second question using the navigator function method. Their setup involved all 19 four-point correlation functions of external operators σ, σ', and ε, where σ and σ' are the two relevant scalar primaries in the fundamental irrep, while ε is the relevant scalar singlet (assumed to be the only relevant scalars in these irreps). Chester and Su's theory space had ten parameters: three scaling dimensions of σ, σ', and ε, and seven ratios of the OPE coefficients among them. Using the Delaunay triangulation-cutting-surface algorithm, they found a cone-shaped allowed region in the space of $(\Delta_\sigma, \Delta_{\sigma'}, \Delta_\varepsilon)$ and identified the three-state Potts CFT with the sharp tip of this region; see Fig. 10.

Chester and Su (2022) proposed a similar identification for the tricritical three-state Potts CFT using a navigator function setup involving the second relevant singlet scalar ε' and a subset of 21 four-point correlation functions involving $\sigma, \sigma', \varepsilon$, and ε'. In $d = 2$ and at $\Lambda = 11$, both identifications agree well with the exact solution.

[28]A related problem is to keep $d = 3$ fixed while varying q. The critical and tricritical q-state Potts CFTs should then merge and annihilate at some $q_c < 3$. Old Monte Carlo simulations suggest that $q_c \approx 2.45$ (Lee and Kosterlitz, 1991).

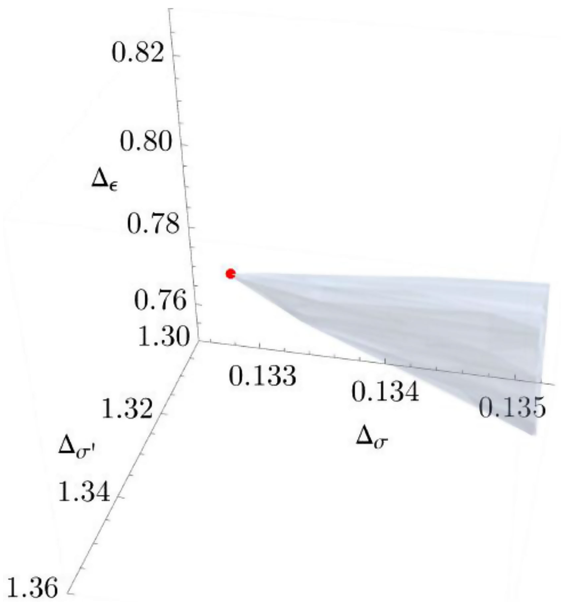

FIG. 10. Cone-shaped allowed region in the space of $(\Delta_\sigma, \Delta_{\sigma'}, \Delta_\varepsilon)$ in $d = 2$ and $\Lambda = 11$ whose tip (red dot) closely agrees with the exact solution of the critical three-state Potts model (Chester and Su, 2022).

Inspired by this agreement, using the navigator function setups, Chester and Su (2022) tried to track the critical and tricritical CFTs as a function of $d > 2$ while assuming the same identification as in $d = 2$. They wanted to see if the two CFTs would come together and merge. Their results were not fully satisfactory. First, while the tricritical scaling dimensions varied continuously, the critical dimensions experienced an unexpected discontinuous jump at $d \approx 2.03$. Second, focusing on the cleaner tricritical curve, one could hope to detect d_c as the point where $\Delta_{\varepsilon'}(d) = d$. On general grounds one would expect a square-root behavior near this crossing (Gorbenko, Rychkov, and Zan, 2018a),

$$\Delta_{\varepsilon'}(d) - d_c \propto \sqrt{d_c - d} \quad (d_c - d \ll 1). \tag{20}$$

Instead, Chester and Su (2022) observed the behavior in Fig. 11. We see that $\Delta_{\varepsilon'}$ starts approaching the $\Delta = d$ line according to the square-root law, but at around $d \sim 2.28$ the behavior crosses over to a linear approach.

To overcome these difficulties, it would be desirable to find a bootstrap setup where the critical and tricritical CFTs would be isolated into islands. Then d_c could be determined from the disappearance of the islands. However, such a setup remains elusive.

VII. `skydive`

In this section we describe `skydive` (Su, 2022a; Liu *et al.*, 2023), the latest dramatic improvement in the series of numerical conformal bootstrap technology improvements that started with the introduction of the navigator function.

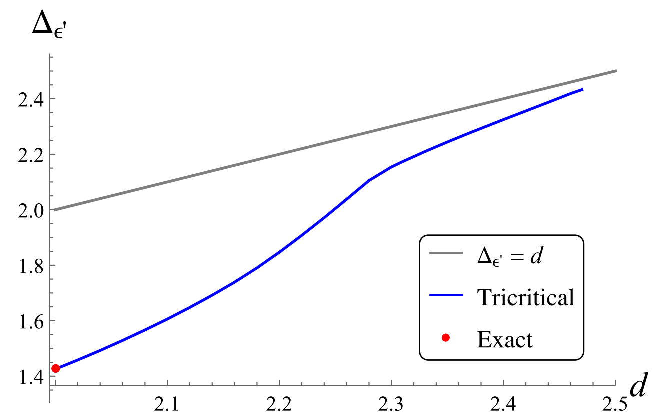

FIG. 11. Tricritical $\Delta_{\varepsilon'}$ as a function of d as extracted by Chester and Su (2022).

A. Basic idea

The typical procedure in navigator computation involves the following steps: (1) select a point in the parameter space and generate the corresponding SDP, (2) compute the SDP to obtain the navigator function and its gradient, (3) make a move in the parameter space based on the local information from the navigator function, and then repeat the process. In step (2), the SDP needs to be fully solved. In the technical terminology of the SDP algorithm realized in `SDPB` (Simmons-Duffin, 2015), an SDP is considered solved when an internal parameter μ, which can be interpreted as an error measure, is reduced below a certain threshold, typically 10^{-30}. Hot starting often leads to the stalling of the solver if the checkpoint has a small μ parameter.[29] A robust strategy avoids hot starting.[30] A typical navigator run spends most of its time computing SDPs.

The basic idea of `skydive` is to optimize this approach using the intuition that an SDP does not need to be completely solved to obtain a rough estimate of the navigator function value. Indeed, a good estimation of the navigator function can be achieved at a finite μ, and such information is sufficient to indicate a good move in theory space. An ideal scenario is as follows: when the solver is far from the final optimal point, it computes the SDP until the μ is small enough to provide a reliable estimation of the navigator function, yet not so small as to cause stalling during hot starting. Based on this estimation, the solver then moves to a new SDP nearby in the parameter space and initiates the computation of this new SDP with the previous checkpoint. In the new computation, only a few iterations are needed to obtain an acceptable estimate of the navigator function since the checkpoint is essentially almost correct. As the solver progresses toward the final optimal point, we should methodically decrease μ to refine the estimates of the navigator function, eventually

[29]This is not surprising, since SDPB uses an interior-point algorithm, which moves through the interior of the allowed region to reach the optimal point on its boundary.

[30]One could attempt to save a checkpoint when μ is not too small. Although the stalling problem is usually less severe in that case, there is still no guarantee that stalling will not occur.

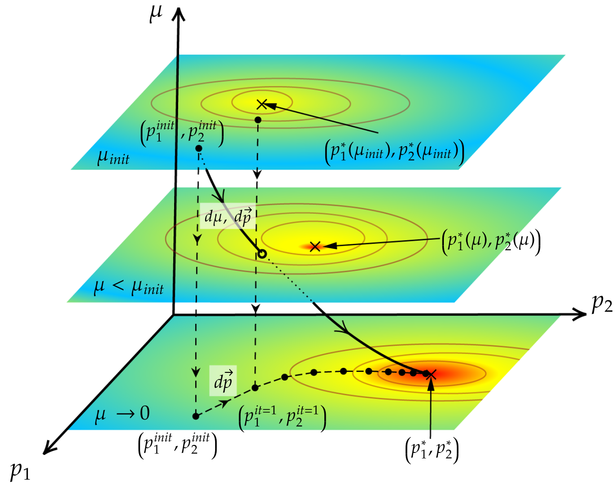

FIG. 12. The original navigator function method compared to the skydiving algorithm. The goal is to minimize the navigator function $\mathcal{N}(p)$, where $p = (p_1, p_2)$ represents the parameters in theory space. In the original navigator method, we solve an SDP at fixed (p_1, p_2) to get $\mathcal{N}(p)$ at $\mu = 0$ following the vertical dashed path. Then we update (p_1, p_2) (as suggested by the BFGS algorithm), compute another SDP starting at $\mu_{\rm init}$, and repeat the process. Instead, `skydive` changes p and μ simultaneously, as depicted by the solid black path, allowing the algorithm to converge to the same navigator minimum. From Liu *et al.*, 2023.

converging on the optimal point with μ below the threshold. This ideal scenario is illustrated in Fig. 12.

B. Algorithm

We now describe the skydiving algorithm that realizes this idea (Liu *et al.*, 2023), which dramatically accelerates navigator-type computations. The skydiving algorithm can be understood as an upgrade of the primal-dual interior-point algorithm used in SDPB. We begin with a summary of the latter. The SDP can be formulated using the Lagrange function as

$$L_\mu(x, y, X, Y) = c^T x + b^T y - x^T B y + \mathrm{Tr}[(X - x^T A_*)Y] - \mu \log\ \det X, \quad (21)$$

where $X, Y \in \mathcal{S}^K$ (symmetric $K \times K$ matrices), $A_* = (A_1, \ldots, A_P) \in (\mathcal{S}^K)^P$, $B \in (\mathbb{R}^n)^P$ are rectangular $n \times P$ matrices, and $c, x \in \mathbb{R}^P$ and $b, y \in \mathbb{R}^n$ are vectors. In bootstrap applications the constant b, c, B, and A quantities are related to the bootstrap conditions and conformal blocks following the procedure of Simmons-Duffin (2015). In this formalism the SDP consists in finding the stationary point[31] of L_μ as $\mu \to 0$, subject to $X, Y \succeq 0$. The last term of Eq. (21) represents a barrier function that pushes us to the interior of the set $X, Y \succeq 0$. This barrier function disappears when the limit $\mu \to 0$ is taken. The primal-dual interior-point algorithm solves the SDP using a variant of the Newton method with two tweaks: (1) To approach the limit $\mu \to 0$, it gradually decreases μ by replacing $\mu \to \beta\mu$ in each iteration of the Newton method with $0 < \beta < 1$. (2) In each step, if the standard Newton steps dX and dY violate the condition $X + dX, Y + dY \succeq 0$, the algorithm performs a partial Newtonian step, rescaling dX and dY with a factor $0 < \alpha < 1$, to ensure that the positive semidefiniteness of X and Y is preserved.

The user-chosen parameter β is important. If β is too small, there is a risk of *stalling*, a phenomenon where α decreases to 0, so the steps become shorter and shorter while the solver is not at the optimal solution. Stalling indicates that the solver is too close to the boundary of the region $X, Y \succeq 0$. On this boundary we have $\det(X) = 0$ and $\det(Y) = 0$. If μ is not sufficiently small, movement toward optimality is severely constrained by being close the boundary. As mentioned in Sec. VII.A, stalling also frequently occurs when hot-starting a new SDP (i.e., initializing the solver with given x, y, X, and Y) using a checkpoint at small μ. This is because one of the stationary conditions is $XY = \mu I$. As $\mu \to 0$, $XY \to 0$ and X and Y become degenerate. From the perspective of the new SDP, the checkpoint is positioned too close to the degeneracy surface, while the solution is far from optimal in the new SDP.

Suppose next that we have a family of SDP depending on a parameter p (which may be multidimensional). For a fixed p the SDP encodes the computation of a navigator function $\mathcal{N}(p)$, which we want to minimize. This means that we aim to perform optimization not only in x, y, X, and Y but also in p. We thus extend the Lagrange function to depend also on p,

$$L_\mu(x, y, X, Y, p) = c^T(p)x + b^T(p)y - x^T B(p)y + \mathrm{Tr}[(X - x^T A_*)Y] - \mu \log \det X. \quad (22)$$

One might hope to follow the same idea as in the primal-dual interior-point algorithm, i.e., using the Newton method in the space of (x, y, X, Y, p) and gradually decreasing μ. However, this naive approach does not work due to much different roles played by x, y, X, and Y than by p: (1) In practical conformal bootstrap applications, the dimensions of x, y, X, and Y are usually much larger than those of p. (2) The Lagrange function depends on x, y, X, and Y in a smooth and convex way, but the dependence on p does not have to be convex. In fact, it is known that the navigator function can exhibit nonconvexity (away from its minimum) and even nonsmoothness. If one does try a naive Newton step treating x, y, X, Y, and p on equal footing, performance is poor. As the solver moves through a rough landscape in p, fixing a constant decreasing rate β is a bad idea and often leads to stalling. And when x, y, X, and Y are not stationary at a fixed p and μ, the predicted step in (x, y, X, Y, p) is often inaccurate.

Overcoming these difficulties required several new ideas that were introduced by Liu *et al.* (2023). (1) The solver dynamically determines a β based on the likelihood of stalling and may even temporarily increase μ (i.e., we use $\beta > 1$) when facing a higher risk of stalling. (2) The solver first finds a stationary solution for x, y, X, and Y at a fixed p and μ. Only then does it perform a Newton step in p. In other words, it attempts to optimize the "finite-μ navigator function," which is defined as $N(p, \mu) = L_\mu(x^*, y^*, X^*, Y^*, p)$, where x^*, y^*, X^*, Y^*

[31]The stationary solution is defined to be a solution to $\partial L/\partial\xi = 0$ for $\xi = x$, y, X, and Y.

represents the stationary solution for a given p and μ. Since the dimension of p is not too large in practice, the latter optimization is much more manageable than the optimization of $L_\mu(x, y, X, Y, p)$. Moreover, solving the stationary solution for x, y, X, and Y at a fixed p and μ is inexpensive. Liu *et al.* (2023) developed a technique that accelerates this part of the computation, typically requiring fewer than four Newton iterations to find a solution with the desired accuracy.

The previous discussion would apply generically when one extremizes within a family of SDPs. However, additional difficulties arise when specializing to conformal bootstrap problems. A notable feature of the navigator function in typical conformal bootstrap studies is that it is fairly flat within the bootstrap island. The gradient inside and outside the island can differ by many orders of magnitude. This feature already poses a challenge[32] in the applications of the navigator function using the original method of Reehorst *et al.* (2021). For the skydiving algorithm this feature would pose a serious challenge in finding the boundary of an island because the Lagrange function will not detect the island (defined by $L < 0$) until μ is small enough, contrary to the general idea of the skydiving algorithm to move toward the optimal point at relatively large μ. To overcome this challenge, Liu *et al.* (2023) proposed a modification of the Lagrangian (22) at $\mu > 0$, which leads to the same allowed island and the same navigator minimum as $\mu \to 0$ but speeds up the optimization algorithm. This modification worked well in the tested examples. See Liu *et al.* (2023) for details.

Liu *et al.* (2023) tested the skydiving algorithm on two previously studied problems involving multiple four-point functions: the 3D Ising correlators of σ, ϵ, and the $\mathrm{O}(3)$ model correlators of the lowest vector, singlet, and rank-2 tensor primaries. The results showed that the skydiving algorithm improved computational efficiency in these examples compared to use of the navigator function without hot starting by factors of 10–100.

The skydiving algorithm has already been used in several bootstrap studies. Notably Rong and Su (2023) investigated the $\mathrm{O}(3)$-symmetric correlators of v (vector), s (singlet), and t_2 and t_4 scalar primaries (where t_k is a traceless symmetric k-index irrep). The information extracted from this computation was used to perform conformal perturbation theory around the $\mathrm{O}(3)$ fixed point to predict the critical exponents of the cubic fixed point. Rong and Su also numerically confirmed the large charge expansion prediction $\Delta_{Q,l} = c_{3/2}Q^{3/2} + c_{1/2}Q^{1/2} - 0.094 + \sqrt{l(l+1)/2}$ (Hellerman *et al.*, 2015; Monin *et al.*, 2017), including for the first time the spin dependent term comparing $l = 0$ and 2. The setup of Rong and Su (2023) involved the largest number of crossing equations ever explored using the numerical bootstrap: 82 equations. The computations were completed in about ten days with the skydiving algorithm. In comparison, it would have taken more than a year using the original navigator function method of Reehorst *et al.* (2021) (without hot starting).

[32]For example, Su (2022b) discussed a situation where the ordinary BFGS algorithm could not effectively handle the sudden change in the order of magnitude of the gradient, and it had to be modified to be efficient.

Another application of `skydive` was given by Chester and Su (2024), which considered SO(5)-symmetric four-point functions of v, s, and t_2 to investigate the scenario where DQCP is governed by a tricritical point corresponding to a unitary CFT; see Sec. III.B.2.

Finally, Reehorst *et al.* (2024) recently used `skydive` to study multiscalar CFTs with $\mathrm{O}(N) \times \mathrm{O}(2)$ global symmetry. They used `skydive` to find the minimal value of the parameter N beyond which the unitary $\mathrm{O}(N) \times \mathrm{O}(2)$ symmetric fixed point ceases to exist.

The skydiving algorithm has created new opportunities in the numerical conformal bootstrap. The algorithm of Liu *et al.* (2023) represented the first attempt at efffective optimization in the x, y, X, Y, and p space. Although the algorithm worked for the tested examples, its robustness needs further study,[33] and future improvements are welcome.

VIII. OMISSIONS

In our review we could not describe or mention every numerical conformal bootstrap result obtained since the previous review by Poland, Rychkov, and Vichi (2019). Notable omissions include work on boundary CFTs (Behan *et al.*, 2022, 2020), solutions of the truncated bootstrap equations [Gliozzi's method (Gliozzi, 2013)] in situations where there is no positivity for four-point functions (Rong and Zhu, 2020; Nakayama, 2021) and for five-point functions (Poland, Prilepina, and Tadić, 2023), work on superconformal field theories (Liendo, Meneghelli, and Mitev, 2018; Lin *et al.*, 2019; Agmon, Chester, and Pufu, 2020; Gimenez-Grau and Liendo, 2020, 2021; Binder *et al.*, 2021; Bissi, Manenti, and Vichi, 2021; Bissi *et al.*, 2022; Chen *et al.*, 2023; Chester, 2023; Chester, Dempsey, and Pufu, 2023), conformal bootstrap in situations where the spectrum is known but OPE coefficients need to be determined (Picco, Ribault, and Santachiara, 2019; Nivesvivat and Ribault, 2021; Cavaglià *et al.*, 2022a, 2022b; Grans-Samuelsson *et al.*, 2022; Niarchos *et al.*, 2023; Ribault, 2023), bounds on CFT correlators (Paulos and Zheng, 2022), work on other numerical methods such as the extremal flow method (Afkhami-Jeddi, 2022), outer approximation and the analytic functional basis (Landry, 2022; Ghosh and Zheng, 2023), machine learning bootstrap (Kántor, Niarchos, and Papageorgakis, 2022; Lal, Majumder, and Sobko, 2023), and stochastic optimization (Laio, Valenzuela, and Serone, 2022; Luviano and Adrian, 2022). We also could not describe the work in the following closely related fields: the modular bootstrap for 2D CFTs (Bae, 2019; Bae, Lee, and Song, 2019; Hartman, Mazáč, and Rastelli, 2019; Huang, Li, and Lin, 2019; Lin and Shao, 2019; 2021, 2023; Afkhami-Jeddi *et al.*, 2020; Benjamin and Lin, 2020; Grigoletto, 2021; Benjamin and Chang, 2022; Chiang *et al.*, 2023; Collier, Mazac, and Wang, 2023; Fitzpatrick and Li, 2023; Grigoletto and Putrov,

[33]The navigator functions for different bootstrap setups may have different features. Some might be more singular than others. Some might have multiple local minima. The difficulty of the optimization also depends on the initial point. We therefore feel that the skydiving algorithm requires more testing in various scenarios.

2023; Lanzetta and Fidkowski, 2023) and the bootstrap for Laplacian eigenvalues on surfaces (Bonifacio, 2022a, 2022b; Bonifacio and Hinterbichler, 2020; Kravchuk, Mazac, and Pal, 2021; Bonifacio, Mazac, and Pal, 2023; Gesteau *et al.*, 2023) [as first shown by Kravchuk, Mazac, and Pal (2021), for hyperbolic surfaces this is extremely closely related to the conformal bootstrap). We could not describe significant progress being achieved in the sister field of the numerical *S*-matrix bootstrap (Kruczenski, Penedones, and Rees, 2022). In addition, several other "bootstraps" use positivity to get bounds on spaces of solutions (although the analogy with the conformal bootstrap is less complete due to the absence of analogs of families of conformal blocks). Those subjects deserve separate reviews, but we now list a few entry points into the literature regarding the lattice model bootstrap (Anderson and Kruczenski, 2017; Cho *et al.*, 2022; Kazakov and Zheng, 2023), the matrix model bootstrap (Lin, 2020; Kazakov and Zheng, 2022), and the quantum mechanics bootstrap (Han, Hartnoll, and Kruthoff, 2020; Lin, 2023).

IX. DISCUSSION AND OUTLOOK

In this review we have covered some advances in numerical conformal bootstrap techniques over the past few years. The development of highly efficient software for computing conformal blocks, effectively solving SDPs, and search algorithms in theory space has been fruitful. With this progress in numerics, much interesting work has been done. In particular, 3D super-Ising, O(2), O(3), and GNY models have been solved to obtain high-precision critical exponents with rigorous error bars.

Many questions remain to be investigated in the future. There are many CFT targets that we would like to solve. How can we bootstrap critical gauge theories to obtain precise CFT data? Which correlators are the most constraining? How to numerically explore correlators that involve Wilson lines? How can we bootstrap multiscalar CFTs beyond the Ising and Ising-like theories? What are the most effective gap assumptions? Can we bootstrap complex CFTs? These are still open questions.

These questions are open even for the 2D minimal models. Can we find a systematic way to constrain minimal models into small bootstrap islands? If so, we might hope to extend these islands into noninteger dimensions $d > 2$.

To bootstrap these and other targets of interest, it is likely that we will need to further develop the bootstrap machinery to make it even more powerful. Given a set of correlators, can we make the bootstrap bound converge faster? This question is especially crucial for correlators of large dimension operators (as is the case for critical gauge theories) since they often converge slowly in the current computational framework. There are several possibilities for acceleration.

- We may hope to accelerate the higher Λ computation with information from a lower Λ computation. This has been employed in the 2D chiral modular bootstrap and has achieved impressive acceleration in computation (Afkhami-Jeddi, Hartman, and Tajdini, 2019).
- In various limits analytic understandings of the spectrum have been achieved, such as the light cone limit and the large charge limit for $\mathrm{O}(N)$. Combining this analytic information with numerical bootstrap technology should further strengthen the constraining power. A nonrigorous "hybrid bootstrap" method to combine the numerical and light cone information was explored by Su (2022b). It would be interesting to explore more robust and rigorous methods.
- There are bases other than the derivative basis that could converge faster. Through use of a better basis, notable improvement has been achieved in the 1D CFT (Paulos and Zan, 2020; Ghosh, Kaviraj, and Paulos, 2021) and 2D CFT cases (Ghosh and Zheng, 2023). In particular, in the latter work the researchers observed that the bound at large external dimensions converges significantly faster than with the derivative basis. Overcoming the remaining challenges to extend this method to three dimensions would be useful for bootstrapping the previously mentioned targets.

We remain optimistic that numerical bootstrap technology will continue to see significant improvement in the future, and we hope that these advancements will continue to yield interesting insights into physics questions.

ACKNOWLEDGMENTS

We thank the numerical conformal bootstrap community for the collective effort that led to the development of the ideas and results presented in this review. We are particularly grateful to our collaborators Shai Chester, Yin-Chen He, Aike Liu, Junyu Liu, Walter Landry, David Poland, Junchen Rong, Marten Reehorst, David Simmons-Duffin, Benoit Sirois, Balt van Rees, and Alessandro Vichi. We thank David Simmons-Duffin for communications about the `tiptop` algorithm, and Johan Henriksson and Stefanos Kousvos for discussions and comments. S. R. is supported by Simons Foundation Grant No. 733758 (Simons Collaboration on the Nonperturbative Bootstrap). Most of N. S.'s work was conducted at the University of Pisa, where this project has received funding from the European Research Council (ERC) under the European Union's Horizon 2020 research and innovation program (Grant Agreement No. 758903). N. S.'s work at the California Institute of Technology is supported in part by Simons Foundation Grant No. 488657 (Simons Collaboration on the Nonperturbative Bootstrap).

APPENDIX: COMMENT ON ISLANDS, ISOLATED REGIONS, AND KINKS

In this review, we use *island*, *isolated or closed regions*, and *kinks* to describe various bootstrap results. We now clarify how we use those terms.

We call an isolated allowed region in the CFT parameter space a bootstrap island of theory X if it satisfies the following conditions: (1) The gap assumptions are mild (i.e., not too close to the actual value in theory X) and/or naturally motivated (for example, by the number of relevant operators, by equations of motion creating gaps in the spectrum, etc). (2) The isolated region is insensitive to the gap assumptions, i.e., the region does not change much if the gaps are varied slightly. (3) The isolated region is small enough that it does not contain any known theories other than X. For example, we consider the 3D Ising CFT island of Kos *et al.* (2016) to satisfy these conditions. When a bootstrap island is obtained, we can often determine some CFT data with more or less rigorous error bars by scanning over the island. One of the main goals of the conformal bootstrap program is to find the correct setups to isolate various CFTs into islands.

Kinks are sudden changes of the slope of the boundary of a feasible region. We call a kink a stable kink of theory X because (1) the gap assumptions leading to the kink are mild and naturally motivated, and (2) the location of the kink is insensitive to the gap assumptions and is consistent with what is known or conjectured about the position of theory X. For example, the kink discussed by El-Showk *et al.* (2012) is a stable 3D Ising CFT kink because, when the gap changes slightly, the location remains the same, although the sharpness of the kink may change. With a stable kink, we could often make predictions on some CFT data, although the error bars may not be as rigorous as with the islands. One sometimes observes *moving kinks*, whose location changes with the gap assumptions (such as the example discussed in Sec. III.B.2). They are less useful than the stable kinks but are not useless. Indeed, in some examples when a certain gap is set to the actual CFT value, the CFT is expected to precisely saturate the kink's moving position. In these cases bootstrap computation could make predictions on CFT data once a few pieces of information obtained using other methods are injected.

Be careful when considering large-N CFT islands. Different CFTs could have the same CFT data in the $N \to \infty$ limit. Therefore, in the theory space there could be multiple solutions that are close to each other at large N, which may not be easily distinguishable via numerical bootstrap analysis. These solutions may show a significant split when N becomes small. Consequently, apparent success at large N does not automatically translate to success at smaller N. For example, in the case of the bosonic QED_3 feasible region given by He, Rong, and Su (2021a), the region is closed for sufficiently large N, but not at small N. It is unclear whether this is due purely to a convergence issue[34] or whether there are several CFTs satisfying the imposed conditions.

Even though the ultimate goal of the conformal bootstrap program is to solve CFTs, for many target theories it is not yet clear how to obtain islands or stable kinks. In such cases people compute generic bounds, while the target CFTs are not on the boundary of the bounds. These bootstrap bounds are also valuable since sufficiently strong bounds could offer insights into related physics questions [as in the case of the DQCP, which was reviewed by Poland, Rychkov, and Vichi (2019)].

[34]It is known that convergence in Λ is slow for correlators of operators with large scaling dimensions, which is the case here.

REFERENCES

Afkhami-Jeddi, Nima, 2022, “Conformal bootstrap deformations,” J. High Energy Phys. 09, 225.

Afkhami-Jeddi, Nima, Henry Cohn, Thomas Hartman, David de Laat, and Amirhossein Tajdini, 2020, “High-dimensional sphere packing and the modular bootstrap,” J. High Energy Phys. 12, 066.

Afkhami-Jeddi, Nima, Thomas Hartman, and Amirhossein Tajdini, 2019, “Fast conformal bootstrap and constraints on 3d gravity,” J. High Energy Phys. 05, 087.

Agmon, Nathan B., Shai M. Chester, and Silviu S. Pufu, 2020, “The M-theory archipelago,” J. High Energy Phys. 02, 010.

Aharony, A., O. Entin-Wohlman, and A. Kudlis, 2022, “Different critical behaviors in cubic to trigonal and tetragonal perovskites,” Phys. Rev. B **105**, 104101.

Aharony, Amnon, 1973, “Critical behavior of anisotropic cubic systems,” Phys. Rev. B **8**, 4270–4273.

Aharony, Ofer, Steven S. Gubser, Juan Martin Maldacena, Hirosi Ooguri, and Yaron Oz, 2000, “Large N field theories, string theory and gravity,” Phys. Rep. **323**, 183–386.

Albayrak, Soner, Rajeev S. Erramilli, Zhijin Li, David Poland, and Yuan Xin, 2022, “Bootstrapping $N_f = 4$ conformal QED_3,” Phys. Rev. D **105**, 085008.

Anderson, Peter D., and Martin Kruczenski, 2017, “Loop equations and bootstrap methods in the lattice,” Nucl. Phys. **B921**, 702–726.

Atanasov, Alexander, Aaron Hillman, and David Poland, 2018, “Bootstrapping the minimal 3D SCFT,” J. High Energy Phys. 11 140.

Atanasov, Alexander, Aaron Hillman, David Poland, Junchen Rong, and Ning Su, 2022, “Precision bootstrap for the $\mathcal{N} = 1$ super-Ising model,” J. High Energy Phys. 08, 136.

Bae, Jin-Beom, 2019, “Constraining two dimensional CFTs with modular invariance,” Proc. Sci. ICHEP2018, 318.

Bae, Jin-Beom, Sungjay Lee, and Jaewon Song, 2019, “Modular constraints on superconformal field theories,” J. High Energy Phys. 01, 209.

Bashkirov, Denis, 2013, “Bootstrapping the $\mathcal{N} = 1$ SCFT in three dimensions,” arXiv:1310.8255.

Behan, Connor, 2017, “`PyCFTBoot`: A flexible interface for the conformal bootstrap,” Commun. Comput. Phys. **22**, 1–38.

Behan, Connor, 2018, “Conformal manifolds: ODEs from OPEs,” J. High Energy Phys. 03, 127.

Behan, Connor, 2019, “Bootstrapping the long-range Ising model in three dimensions,” J. Phys. A **52**, 075401.

Behan, Connor, Lorenzo Di Pietro, Edoardo Lauria, and Balt C. van Rees, 2020, “Bootstrapping boundary-localized interactions,” J. High Energy Phys. 12, 182.

Behan, Connor, Lorenzo Di Pietro, Edoardo Lauria, and Balt C. van Rees, 2022, “Bootstrapping boundary-localized interactions II. Minimal models at the boundary,” J. High Energy Phys. 03, 146.

Behan, Connor, Peter Kravchuk, Walter Landry, and David Simmons-Duffin, 2019, computer code `scalar_blocks`, https://gitlab.com/bootstrapcollaboration/scalar_blocks.

Behan, Connor, Edoardo Lauria, Maria Nocchi, and Philine van Vliet, 2023, “Analytic and numerical bootstrap for the long-range Ising model,” arXiv:2311.02742.

Belavin, A. A., Alexander M. Polyakov, and A. B. Zamolodchikov, 1984, “Infinite conformal symmetry in two-dimensional quantum field theory,” Nucl. Phys. **B241**, 333–380.

Benjamin, Nathan, and Cyuan-Han Chang, 2022, “Scalar modular bootstrap and zeros of the Riemann zeta function,” J. High Energy Phys. 11, 143.

Benjamin, Nathan, and Ying-Hsuan Lin, 2020, "Lessons from the Ramond sector," SciPost Phys. **9**, 065.

Binder, Damon J., Shai M. Chester, Max Jerdee, and Silviu S. Pufu, 2021, "The 3d $\mathcal{N}=6$ bootstrap: From higher spins to strings to membranes," J. High Energy Phys. 05, 083.

Bissi, Agnese, Francesco Fucito, Andrea Manenti, José Francisco Morales, and Raffaele Savelli, 2022, "OPE coefficients in Argyres-Douglas theories," J. High Energy Phys. 06, 085.

Bissi, Agnese, Andrea Manenti, and Alessandro Vichi, 2021, "Bootstrapping mixed correlators in $\mathcal{N}=4$ super Yang-Mills," J. High Energy Phys. 05, 111.

Bissi, Agnese, Aninda Sinha, and Xinan Zhou, 2022, "Selected topics in analytic conformal bootstrap: A guided journey," Phys. Rep. **991**, 1–89.

Bonanno, Claudio, Andrea Cappelli, Mikhail Kompaniets, Satoshi Okuda, and Kay Jörg Wiese, 2023, "Benchmarking the Ising universality class in $3 \leq d < 4$ dimensions," SciPost Phys. **14**, 135.

Bonifacio, James, 2022a, "Bootstrap bounds on closed hyperbolic manifolds," J. High Energy Phys. 02, 025.

Bonifacio, James, 2022b, "Bootstrapping closed hyperbolic surfaces," J. High Energy Phys. 03, 093.

Bonifacio, James, and Kurt Hinterbichler, 2020, "Bootstrap bounds on closed Einstein manifolds," J. High Energy Phys. 10, 069.

Bonifacio, James, Dalimil Mazac, and Sridip Pal, 2023, "Spectral bounds on hyperbolic 3-manifolds: Associativity and the trace formula," arXiv:2308.11174.

Cappelli, Andrea, Lorenzo Maffi, and Satoshi Okuda, 2019, "Critical Ising model in varying dimension by conformal bootstrap," J. High Energy Phys. 01, 161.

Cardy, John L., 1987, "Conformal invariance," in *Phase Transitions and Critical Phenomena*, Vol. 11, edited by C. M. Domb and M. S. Green (Academic Press, New York), pp. 55–126.

Cavaglià, Andrea, Nikolay Gromov, Julius Julius, and Michelangelo Preti, 2022a, "Bootstrability in defect CFT: Integrated correlators and sharper bounds," J. High Energy Phys. 05, 164.

Cavaglià, Andrea, Nikolay Gromov, Julius Julius, and Michelangelo Preti, 2022b, "Integrability and conformal bootstrap: One dimensional defect conformal field theory," Phys. Rev. D **105**, L021902.

Chen, Bin-Bin, Xu Zhang, and Zi Yang Meng, 2024, "Emergent conformal symmetry at the multicritical point of $(2+1)$D SO(5) model with Wess-Zumino-Witten term on sphere," arXiv:2405.04470.

Chen, Bin-Bin, Xu Zhang, Yuxuan Wang, Kai Sun, and Zi Yang Meng, 2023, "Phases of $(2+1)$D SO(5) non-linear sigma model with a topological term on a sphere: Multicritical point and disorder phase," arXiv:2307.05307.

Chester, Shai M., 2023, "Bootstrapping 4d $\mathcal{N}=2$ gauge theories: The case of SQCD," J. High Energy Phys. 01, 107.

Chester, Shai M., Ross Dempsey, and Silviu S. Pufu, 2023, "Bootstrapping $\mathcal{N}=4$ super-Yang-Mills on the conformal manifold," J. High Energy Phys. 01, 038.

Chester, Shai M., Luca V. Iliesiu, Mark Mezei, and Silviu S. Pufu, 2018, "Monopole operators in U(1) Chern-Simons-Matter theories," J. High Energy Phys. 05, 157.

Chester, Shai M., Walter Landry, Junyu Liu, David Poland, David Simmons-Duffin, Ning Su, and Alessandro Vichi, 2021, "Bootstrapping Heisenberg magnets and their cubic instability," Phys. Rev. D **104**, 105013.

Chester, Shai M., Walter Landry, Junyu Liu, David Poland, David Simmons-Duffin, Ning Su, and Alessandro Vichi, 2020, "Carving out OPE space and precise O(2) model critical exponents," J. High Energy Phys. 06, 142.

Chester, Shai M., and Silviu S. Pufu, 2016, "Towards bootstrapping QED_3," J. High Energy Phys. 08, 019.

Chester, Shai M., and Ning Su, 2022, "Upper critical dimension of the 3-state Potts model," arXiv:2210.09091.

Chester, Shai M., and Ning Su, 2024, "Bootstrapping Deconfined Quantum Tricriticality," Phys. Rev. Lett. **132**, 111601.

Chiang, Li-Yuan, Tzu-Chen Huang, Yu-tin Huang, Wei Li, Laurentiu Rodina, and He-Chen Weng, 2023, "The geometry of the modular bootstrap," arXiv:2308.11692.

Cho, Minjae, Barak Gabai, Ying-Hsuan Lin, Victor A. Rodriguez, Joshua Sandor, and Xi Yin, 2022, "Bootstrapping the Ising model on the lattice," arXiv:2206.12538.

Collier, Scott, Dalimil Mazac, and Yifan Wang, 2023, "Bootstrapping boundaries and branes," J. High Energy Phys. 02, 019.

Douglas, Michael R., 2013, "Spaces of quantum field theories," J. Phys. Conf. Ser. **462**, 012011.

Dymarsky, Anatoly, Joao Penedones, Emilio Trevisani, and Alessandro Vichi, 2019, "Charting the space of 3D CFTs with a continuous global symmetry," J. High Energy Phys. 05, 098.

El-Showk, Sheer, and Miguel F. Paulos, 2013, "Bootstrapping Conformal Field Theories with the Extremal Functional Method," Phys. Rev. Lett. **111**, 241601.

El-Showk, Sheer, Miguel F. Paulos, David Poland, Slava Rychkov, David Simmons-Duffin, and Alessandro Vichi, 2012, "Solving the 3D Ising model with the conformal bootstrap," Phys. Rev. D **86**, 025022.

El-Showk, Sheer, Miguel F. Paulos, David Poland, Slava Rychkov, David Simmons-Duffin, and Alessandro Vichi, 2014a, "Conformal Field Theories in Fractional Dimensions," Phys. Rev. Lett. **112**, 141601.

El-Showk, Sheer, Miguel F. Paulos, David Poland, Slava Rychkov, David Simmons-Duffin, and Alessandro Vichi, 2014b, "Solving the 3d Ising model with the conformal bootstrap II. c-minimization and precise critical exponents," J. Stat. Phys. **157**, 869.

Erramilli, Rajeev S., Luca V. Iliesiu, and Petr Kravchuk, 2019, "Recursion relation for general 3d blocks," J. High Energy Phys. 12, 116.

Erramilli, Rajeev S., Luca V. Iliesiu, Petr Kravchuk, Walter Landry, David Poland, and David Simmons-Duffin, 2021, "`blocks_3d`: Software for general 3d conformal blocks," J. High Energy Phys. 11, 006.

Erramilli, Rajeev S., Luca V. Iliesiu, Petr Kravchuk, Aike Liu, David Poland, and David Simmons-Duffin, 2023, "The Gross-Neveu-Yukawa archipelago," J. High Energy Phys. 02, 036.

Fitzpatrick, A. Liam, and Wei Li, 2023, "Improving modular bootstrap bounds with integrality," arXiv:2308.08725.

Gesteau, Elliott, Sridip Pal, David Simmons-Duffin, and Yixin Xu, 2023, "Bounds on spectral gaps of hyperbolic spin surfaces," arXiv:2311.13330.

Ghosh, Kausik, Apratim Kaviraj, and Miguel F. Paulos, 2021, "Charging up the functional bootstrap," J. High Energy Phys. 10, 116.

Ghosh, Kausik, and Zechuan Zheng, 2023, "Numerical conformal bootstrap with analytic functionals and outer approximation," arXiv:2307.11144.

Gimenez-Grau, Aleix, and Pedro Liendo, 2020, "Bootstrapping line defects in $\mathcal{N}=2$ theories," J. High Energy Phys. 03, 121.

Gimenez-Grau, Aleix, and Pedro Liendo, 2021, "Bootstrapping Coulomb and Higgs branch operators," J. High Energy Phys. 01, 175.

Gliozzi, Ferdinando, 2013, "More Constraining Conformal Bootstrap," Phys. Rev. Lett. **111**, 161602.

Go, Mocho, 2020, "An automated generation of bootstrap equations for numerical study of critical phenomena," arXiv:2006.04173.

Go, Mocho, and Yuji Tachikawa, 2019, "autoboot: A generator of bootstrap equations with global symmetry," J. High Energy Phys. 06, 084.

Golden, John, and Miguel F. Paulos, 2015, "No unitary bootstrap for the fractal Ising model," J. High Energy Phys. 03, 167.

Gorbenko, Victor, Slava Rychkov, and Bernardo Zan, 2018a, "Walking, weak first-order transitions, and complex CFTs," J. High Energy Phys. 10, 108.

Gorbenko, Victor, Slava Rychkov, and Bernardo Zan, 2018b, "Walking, weak first-order transitions, and complex CFTs II. Two-dimensional Potts model at $Q > 4$," SciPost Phys. **5**, 050.

Gracey, J. A., 2018, "Fermion bilinear operator critical exponents at $O(1/N^2)$ in the QED-Gross-Neveu universality class," Phys. Rev. D **98**, 085012.

Grans-Samuelsson, Linnea, Rongvoram Nivesvivat, Jesper Lykke Jacobsen, Sylvain Ribault, and Hubert Saleur, 2022, "Global symmetry and conformal bootstrap in the two-dimensional $O(n)$ model," SciPost Phys. **12**, 147.

Grigoletto, Andrea, 2021, "Anomalies of fermionic CFTs via cobordism and bootstrap," arXiv:2112.01485.

Grigoletto, Andrea, and Pavel Putrov, 2023, "Spin-cobordisms, surgeries and fermionic modular bootstrap," Commun. Math. Phys. **401**, 3169–3245.

Grover, Tarun, D. N. Sheng, and Ashvin Vishwanath, 2014, "Emergent space-time supersymmetry at the boundary of a topological phase," Science **344**, 280–283.

Gukov, Sergei, 2017, "RG flows and bifurcations," Nucl. Phys. **B919**, 583–638.

Han, Xizhi, Sean A. Hartnoll, and Jorrit Kruthoff, 2020, "Bootstrapping Matrix Quantum Mechanics," Phys. Rev. Lett. **125**, 041601.

Hartman, Thomas, Dalimil Mazáč, David Simmons-Duffin, and Alexander Zhiboedov, 2022, "Snowmass white paper: The analytic conformal bootstrap," in *Proceedings of the 2021 U.S. Community Study on the Future of Particle Physics (Snowmass 2021), 2021*, edited by Joel N. Butler, R. Sekhar Chivukula, and Michael E. Peskin, https://www.slac.stanford.edu/econf/C210711/.

Hartman, Thomas, Dalimil Mazáč, and Leonardo Rastelli, 2019, "Sphere packing and quantum gravity," J. High Energy Phys. 12, 048.

Hasenbusch, Martin, 2019, "Monte Carlo study of an improved clock model in three dimensions," Phys. Rev. B **100**, 224517.

Hasenbusch, Martin, 2023, "Cubic fixed point in three dimensions: Monte Carlo simulations of the $\phi 4$ model on the simple cubic lattice," Phys. Rev. B **107**, 024409.

Hasenbusch, Martin, and Ettore Vicari, 2011, "Anisotropic perturbations in three-dimensional $O(N)$-symmetric vector models," Phys. Rev. B **84**, 125136.

He, Yin-Chen, Junchen Rong, and Ning Su, 2021a, "A roadmap for bootstrapping critical gauge theories: Decoupling operators of conformal field theories in $d > 2$ dimensions," SciPost Phys. **11**, 111.

He, Yin-Chen, Junchen Rong, and Ning Su, 2021b, "Non-Wilson-Fisher kinks of $O(N)$ numerical bootstrap: From the deconfined phase transition to a putative new family of CFTs," SciPost Phys. **10**, 115.

He, Yin-Chen, Junchen Rong, and Ning Su, 2022, "Conformal bootstrap bounds for the $U(1)$ Dirac spin liquid and $N = 7$ Stiefel liquid," SciPost Phys. **13**, 014.

He, Yin-Chen, Junchen Rong, Ning Su, and Alessandro Vichi, 2023, "Non-Abelian currents bootstrap," arXiv:2302.11585.

He, Yin-Chen, Michael P. Zaletel, Masaki Oshikawa, and Frank Pollmann, 2017, "Signatures of Dirac Cones in a DMRG Study of the Kagome Heisenberg Model," Phys. Rev. X **7**, 031020.

Hellerman, Simeon, Domenico Orlando, Susanne Reffert, and Masataka Watanabe, 2015, "On the CFT operator spectrum at large global charge," J. High Energy Phys. 12, 071.

Henriksson, Johan, Stefanos R. Kousvos, and Marten Reehorst, 2023, "Spectrum continuity and level repulsion: The Ising CFT from infinitesimal to finite ε," J. High Energy Phys. 02, 218.

Henriksson, Johan, Stefanos Robert Kousvos, and Andreas Stergiou, 2020, "Analytic and numerical bootstrap of CFTs with $O(m) \times O(n)$ global symmetry in 3D," SciPost Phys. **9**, 035.

Henriksson, Johan, and Andreas Stergiou, 2021, "Perturbative and nonperturbative studies of CFTs with MN global symmetry," SciPost Phys. **11**, 015.

Hermele, Michael, T. Senthil, and Matthew P. A. Fisher, 2005, "Algebraic spin liquid as the mother of many competing orders," Phys. Rev. B **72**, 104404.

Hofman, Diego M., and Juan Maldacena, 2008, "Conformal collider physics: Energy and charge correlations," J. High Energy Phys. 05, 012.

Hogervorst, Matthijs, Slava Rychkov, and Balt C. van Rees, 2015, "Truncated conformal space approach in d dimensions: A cheap alternative to lattice field theory?" Phys. Rev. D **91**, 025005.

Hogervorst, Matthijs, Slava Rychkov, and Balt C. van Rees, 2016, "Unitarity violation at the Wilson-Fisher fixed point in 4-ϵ dimensions," Phys. Rev. D **93**, 125025.

Hu, Shijie, W. Zhu, Sebastian Eggert, and Yin-Chen He, 2019, "Dirac Spin Liquid on the Spin-$1/2$ Triangular Heisenberg Antiferromagnet," Phys. Rev. Lett. **123**, 207203.

Huang, Yu-Tin, Wei Li, and Guan-Lin Lin, 2019, "The geometry of optimal functionals," arXiv:1912.01273.

Huffman, Emilie, and Shailesh Chandrasekharan, 2020, "Fermion-bag inspired Hamiltonian lattice field theory for fermionic quantum criticality," Phys. Rev. D **101**, 074501.

Ihrig, Bernhard, Luminita N. Mihaila, and Michael M. Scherer, 2018, "Critical behavior of Dirac fermions from perturbative renormalization," Phys. Rev. B **98**, 125109.

Iliesiu, Luca, 2018, "Bootstrapping the Néel-VBS quantum phase transition," lecture, Simons Center for Geometry and Physics.

Iliesiu, Luca, Filip Kos, David Poland, Silviu S. Pufu, David Simmons-Duffin, and Ran Yacoby, 2016, "Bootstrapping 3D fermions," J. High Energy Phys. 03, 120.

Janke, Wolfhard, and Ramon Villanova, 1997, "Three-dimensional three state Potts model revisited with new techniques," Nucl. Phys. **B489**, 679–696.

Kadanoff, Leo P., 1969, "Operator Algebra and the Determination of Critical Indices," Phys. Rev. Lett. **23**, 1430–1433.

Kántor, Gergely, Vasilis Niarchos, and Constantinos Papageorgakis, 2022, "Conformal bootstrap with reinforcement learning," Phys. Rev. D **105**, 025018.

Karthik, Nikhil, and Rajamani Narayanan, 2016a, "No evidence for bilinear condensate in parity-invariant three-dimensional QED with massless fermions," Phys. Rev. D **93**, 045020.

Karthik, Nikhil, and Rajamani Narayanan, 2016b, "Scale invariance of parity-invariant three-dimensional QED," Phys. Rev. D **94**, 065026.

Karthik, Nikhil, and Rajamani Narayanan, 2019, "Numerical determination of monopole scaling dimension in parity-invariant three-dimensional noncompact QED," Phys. Rev. D **100**, 054514.

Kazakov, Vladimir, and Zechuan Zheng, 2022, "Analytic and numerical bootstrap for one-matrix model and 'unsolvable' two-matrix model," J. High Energy Phys. 06, 030.

Kazakov, Vladimir, and Zechuan Zheng, 2023, "Bootstrap for lattice Yang-Mills theory," Phys. Rev. D **107**, L051501.

Korchemsky, G. P., 2016, "On level crossing in conformal field theories," J. High Energy Phys. 03, 212.

Kos, Filip, David Poland, and David Simmons-Duffin, 2014a, "Bootstrapping mixed correlators in the 3D Ising model," J. High Energy Phys. 11, 109.

Kos, Filip, David Poland, and David Simmons-Duffin, 2014b, "Bootstrapping the $\mathrm{O}(N)$ vector models," J. High Energy Phys. 06, 091.

Kos, Filip, David Poland, David Simmons-Duffin, and Alessandro Vichi, 2015, "Bootstrapping the $\mathrm{O}(N)$ Archipelago," J. High Energy Phys. 11, 106.

Kos, Filip, David Poland, David Simmons-Duffin, and Alessandro Vichi, 2016, "Precision islands in the Ising and $\mathrm{O}(N)$ models," J. High Energy Phys. 08, 036.

Kousvos, Stefanos R., and Andreas Stergiou, 2019, "Bootstrapping mixed correlators in three-dimensional cubic theories," SciPost Phys. **6**, 035.

Kousvos, Stefanos R., and Andreas Stergiou, 2020, "Bootstrapping mixed correlators in three-dimensional cubic theories II," SciPost Phys. **8**, 085.

Kousvos, Stefanos Robert, and Andreas Stergiou, 2022, "Bootstrapping mixed MN correlators in 3D," SciPost Phys. **12**, 206.

Kousvos, Stefanos Robert, and Andreas Stergiou, 2023, "CFTs with $\mathrm{U}(m)\times\mathrm{U}(n)$ global symmetry in 3D and the chiral phase transition of QCD," SciPost Phys. **15**, 075.

Kravchuk, Petr, Dalimil Mazac, and Sridip Pal, 2021, "Automorphic spectra and the conformal bootstrap," arXiv:2111.12716.

Kruczenski, Martin, Joao Penedones, and Balt C. van Rees, 2022, "Snowmass white paper: S-matrix bootstrap," arXiv:2203.02421.

Laio, Alessandro, Uriel Luviano Valenzuela, and Marco Serone, 2022, "Monte Carlo approach to the conformal bootstrap," Phys. Rev. D **106**, 025019.

Lal, Shailesh, Suvajit Majumder, and Evgeny Sobko, 2023, "The R-mAtrIx net," arXiv:2304.07247.

Landry, Walter, 2022, computer code `outer_limits`, https://github.com/davidsd/sdpb/tree/2.5.0/src/outer_limits.

Landry, Walter, and David Simmons-Duffin, 2019, "Scaling the semidefinite program solver `SDPB`," arXiv:1909.09745.

Lanzetta, Ryan A., and Lukasz Fidkowski, 2023, "Bootstrapping Lieb-Schultz-Mattis anomalies," Phys. Rev. B **107**, 205137.

Lee, Jooyoung, and J. M. Kosterlitz, 1991, "Three-dimensional q-state Potts model: Monte Carlo study near $q=3$," Phys. Rev. B **43**, 1268–1271.

Li, Zhijin, 2022a, "Bootstrapping conformal QED_3 and deconfined quantum critical point," J. High Energy Phys. 11, 005.

Li, Zhijin, 2022b, "Conformality and self-duality of $N_f=2$ QED_3," Phys. Lett. B **831**, 137192.

Li, Zhijin, and David Poland, 2021, "Searching for gauge theories with the conformal bootstrap," J. High Energy Phys. 03, 172.

Liendo, Pedro, Carlo Meneghelli, and Vladimir Mitev, 2018, "Bootstrapping the half-BPS line defect," J. High Energy Phys. 10, 077.

Lin, Henry W., 2020, "Bootstraps to strings: Solving random matrix models with positivity," J. High Energy Phys. 06, 090.

Lin, Henry W., 2023, "Bootstrap bounds on D0-brane quantum mechanics," J. High Energy Phys. 06, 038.

Lin, Ying-Hsuan, David Meltzer, Shu-Heng Shao, and Andreas Stergiou, 2019, "Bounds on triangle anomalies in $(3+1)d$," arXiv:1909.11676.

Lin, Ying-Hsuan, and Shu-Heng Shao, 2019, "Anomalies and bounds on charged operators," Phys. Rev. D **100**, 025013.

Lin, Ying-Hsuan, and Shu-Heng Shao, 2021, "$\mathbb{Z}_N$ symmetries, anomalies, and the modular bootstrap," Phys. Rev. D **103**, 125001.

Lin, Ying-Hsuan, and Shu-Heng Shao, 2023, "Bootstrapping non-invertible symmetries," Phys. Rev. D **107**, 125025.

Lipa, J. A., J. A. Nissen, D. A. Stricker, D. R. Swanson, and T. C. P. Chui, 2003, "Specific heat of liquid helium in zero gravity very near the lambda point," Phys. Rev. B **68**, 174518.

Lipa, J. A., D. R. Swanson, J. A. Nissen, T. C. P. Chui, and U. E. Israelsson, 1996, "Heat Capacity and Thermal Relaxation of Bulk Helium very near the Lambda Point," Phys. Rev. Lett. **76**, 944–947.

Lipa, J. A., D. R. Swanson, J. A. Nissen, Z. K. Geng, P. R. Williamson, D. A. Stricker, T. C. P. Chui, U. E. Israelsson, and M. Larson, 2000, "Specific Heat of Helium Confined to a 57-μm Planar Geometry near the Lambda Point," Phys. Rev. Lett. **84**, 4894–4897.

Liu, Aike, David Simmons-Duffin, Ning Su, and Balt C. van Rees, 2023, "Skydiving to bootstrap islands," arXiv:2307.13046.

Liu, Junyu, David Meltzer, David Poland, and David Simmons-Duffin, 2020, "The Lorentzian inversion formula and the spectrum of the 3d $\mathrm{O}(2)$ CFT," J. High Energy Phys. 09, 115; 01 (2021) 206(E).

Liu, Yuzhi, Wei Wang, Kai Sun, and Zi Yang Meng, 2020, "Designer Monte Carlo simulation for the Gross-Neveu-Yukawa transition," Phys. Rev. B **101**, 064308.

Luty, Markus A., and Takemichi Okui, 2006, "Conformal technicolor," J. High Energy Phys. 09, 070.

Luviano, Valenzuela and Uriel Adrian, 2022, "Stochastic minimization in the conformal bootstrap," Ph.D. thesis [International School for Advanced Studies (SISSA)].

Ma, Ruochen, and Chong Wang, 2020, "Theory of deconfined pseudocriticality," Phys. Rev. B **102**, 020407.

Maldacena, Juan, and Alexander Zhiboedov, 2013, "Constraining conformal field theories with a higher spin symmetry," J. Phys. A **46**, 214011.

Manashov, Alexander N., and Matthias Strohmaier, 2018, "Correction exponents in the Gross-Neveu-Yukawa model at $1/N^2$," Eur. Phys. J. C **78**, 454.

Metlitski, Max A., 2022, "Boundary criticality of the $\mathrm{O}(N)$ model in $d=3$ critically revisited," SciPost Phys. **12**, 131.

Mitchell, Matthew S., and David Poland, 2024, "Bounding irrelevant operators in the 3d Gross-Neveu-Yukawa CFTs," arXiv:2406.12974.

Monin, Alexander, David Pirtskhalava, Riccardo Rattazzi, and Fiona K. Seibold, 2017, "Semiclassics, Goldstone bosons and CFT data," J. High Energy Phys. 06, 011.

Nahum, Adam, 2020, "Note on Wess-Zumino-Witten models and quasiuniversality in $2+1$ dimensions," Phys. Rev. B **102**, 201116.

Nakayama, Yu, 2015, "Scale invariance vs conformal invariance," Phys. Rep. **569**, 1–93.

Nakayama, Yu, 2021, "Is there supersymmetric Lee-Yang fixed point in three dimensions?," Int. J. Mod. Phys. A **36**, 2150176.

Nakayama, Yu, and Tomoki Ohtsuki, 2014, "Approaching the conformal window of $\mathrm{O}(n)\times\mathrm{O}(m)$ symmetric Landau-Ginzburg models using the conformal bootstrap," Phys. Rev. D **89**, 126009.

Nakayama, Yu, and Tomoki Ohtsuki, 2016, "Conformal Bootstrap Dashing Hopes of Emergent Symmetry," Phys. Rev. Lett. **117**, 131601.

Niarchos, V., C. Papageorgakis, P. Richmond, A. G. Stapleton, and M. Woolley, 2023, "Bootstrability in line-defect CFT with improved truncation methods," arXiv:2306.15730.

Nivesvivat, Rongvoram, and Sylvain Ribault, 2021, "Logarithmic CFT at generic central charge: From Liouville theory to the Q-state Potts model," SciPost Phys. **10**, 021.

Ohtsuki, Tomoki, 2016a, computer code `cboot`, https://github.com/tohtsky/cboot.

Ohtsuki, Tomoki, 2016b, "Applied conformal bootstrap," Ph.D. thesis (University of Tokyo).

Padayasi, Jaychandran, Abijith Krishnan, Max A. Metlitski, Ilya A. Gruzberg, and Marco Meineri, 2022, "The extraordinary boundary transition in the 3d O(N) model via conformal bootstrap," SciPost Phys. **12**, 190.

Paulos, Miguel F., 2014, "JuliBootS: A hands-on guide to the conformal bootstrap," arXiv:1412.4127.

Paulos, Miguel F., and Bernardo Zan, 2020, "A functional approach to the numerical conformal bootstrap," J. High Energy Phys. 09, 006.

Paulos, Miguel F., and Zechuan Zheng, 2022, "Bounding 3d CFT correlators," J. High Energy Phys. 04, 102.

Pelissetto, Andrea, and Ettore Vicari, 2002, "Critical phenomena and renormalization-group theory," Phys. Rep. **368**, 549–727.

Picco, Marco, Sylvain Ribault, and Raoul Santachiara, 2019, "On four-point connectivities in the critical 2d Potts model," SciPost Phys. **7**, 044.

Poland, David, Valentina Prilepina, and Petar Tadić, 2023, "The five-point bootstrap," J. High Energy Phys. 10, 153.

Poland, David, Slava Rychkov, and Alessandro Vichi, 2019, "The conformal bootstrap: Theory, numerical techniques, and applications," Rev. Mod. Phys. **91**, 015002.

Poland, David, and David Simmons-Duffin, 2022, "Snowmass white paper: The numerical conformal bootstrap," in *Proceedings of the 2021 U.S. Community Study on the Future of Particle Physics (Snowmass 2021), 2021*, edited by Joel N. Butler, R. Sekhar Chivukula, and Michael E. Peskin, https://www.slac.stanford.edu/econf/C210711/.

Polchinski, J., 2007, *String Theory. Vol. 1: An Introduction to the Bosonic String* (Cambridge University Press, Cambridge, England).

Polyakov, A. M., 1974, "Non-Hamiltonian approach to conformal quantum field theory," Zh. Eksp. Teor. Fiz. **66**, 23–42, https://inspirehep.net/literature/96660.

Qin, Yan Qi, Yuan-Yao He, Yi-Zhuang You, Zhong-Yi Lu, Arnab Sen, Anders W. Sandvik, Cenke Xu, and Zi Yang Meng, 2017, "Duality between the Deconfined Quantum-Critical Point and the Bosonic Topological Transition Phys. Rev. X **7**, 031052.

Rattazzi, Riccardo, Vyacheslav S. Rychkov, Erik Tonni, and Alessandro Vichi, 2008, "Bounding scalar operator dimensions in 4D CFT," J. High Energy Phys. 12, 031.

Reehorst, Marten, 2022, "Rigorous bounds on irrelevant operators in the 3d Ising model CFT," J. High Energy Phys. 09, 177.

Reehorst, Marten, Maria Refinetti, and Alessandro Vichi, 2023, "Bootstrapping traceless symmetric O(N) scalars," SciPost Phys. **14**, 068.

Reehorst, Marten, Slava Rychkov, David Simmons-Duffin, Benoit Sirois, Ning Su, and Balt van Rees, 2021, "Navigator function for the conformal bootstrap," SciPost Phys. **11**, 072.

Reehorst, Marten, Slava Rychkov, Benoit Sirois, and Balt C. van Rees, 2024, "Bootstrapping frustrated magnets: The fate of the chiral O(N) $\times$ O(2) universality class," arXiv:2405.19411.

Reehorst, Marten, and Benoit Sirois, 2023, "Bootstrapping frustrated magnets: O(N) $\times$ O(2) model," lecture, Bootstrap 2023, Saõ Paulo, 2023, https://www.youtube.com/live/_p1Q4RmTQak?feature=share.

Reehorst, Marten, Emilio Trevisani, and Alessandro Vichi, 2020, "Mixed scalar-current bootstrap in three dimensions," J. High Energy Phys. 12, 156.

Ribault, Sylvain, 2023, "Diagonal fields in critical loop models," SciPost Phys. Core **6**, 020.

Rong, Junchen, and Slava Rychkov, 2023, "Classifying irreducible fixed points of five scalar fields in perturbation theory," arXiv:2306.09419.

Rong, Junchen, and Ning Su, 2018, "Scalar CFTs and their large N limits," J. High Energy Phys. 09, 103.

Rong, Junchen, and Ning Su, 2021a, "Bootstrapping the $\mathcal{N}=1$ Wess-Zumino models in three dimensions," J. High Energy Phys. 06, 153.

Rong, Junchen, and Ning Su, 2021b, "Bootstrapping the minimal $\mathcal{N}=1$ superconformal field theory in three dimensions," J. High Energy Phys. 06, 154.

Rong, Junchen, and Ning Su, 2023, "From O(3) to cubic CFT: Conformal perturbation and the large charge sector," arXiv:2311.00933.

Rong, Junchen, and Jierong Zhu, 2020, "On the ϕ^3 theory above six dimensions," J. High Energy Phys. 04, 151.

Rychkov, Slava, 2020, "Open problems in conformal bootstrap. Problem 1: Bootstrap proof of first-order transitions?," https://sites.google.com/site/slavarychkov/open-problems-in-conformal-bootstrap.

Sachdev, Subir, 2011, *Quantum Phase Transitions*, 2nd ed. (Cambridge University Press, Cambridge, England).

Senthil, T., Leon Balents, Subir Sachdev, Ashvin Vishwanath, and Matthew P. A. Fisher, 2004, "Quantum criticality beyond the Landau-Ginzburg-Wilson paradigm," Phys. Rev. B **70**, 144407.

Senthil, T., Ashvin Vishwanath, Leon Balents, Subir Sachdev, and Matthew P. A. Fisher, 2004, "Deconfined quantum critical points," Science **303**, 1490–1494.

Simmons-Duffin, David, 2015, "A semidefinite program solver for the conformal bootstrap," J. High Energy Phys. 06, 174.

Simmons-Duffin, David, 2016, computer code hyperion, https://github.com/davidsd/hyperion.

Simmons-Duffin, David, 2017, "The lightcone bootstrap and the spectrum of the 3d Ising CFT," J. High Energy Phys. 03, 086.

Sirois, Benoit, 2022, "Navigating through the O(N) archipelago," SciPost Phys. **13**, 081.

Song, Xue-Yang, Yin-Chen He, Ashvin Vishwanath, and Chong Wang, 2020, "From Spinon Band Topology to the Symmetry Quantum Numbers of Monopoles in Dirac Spin Liquids," Phys. Rev. X **10**, 011033.

Song, Xue-Yang, Chong Wang, Ashvin Vishwanath, and Yin-Chen He, 2019, "Unifying description of competing orders in two dimensional quantum magnets," Nat. Commun. **10**, 4254.

Stergiou, Andreas, 2019, "Bootstrapping MN and tetragonal CFTs in three dimensions," SciPost Phys. **7**, 010.

Stergiou, Andreas, 2018, "Bootstrapping hypercubic and hypertetrahedral theories in three dimensions," J. High Energy Phys. 05, 035.

Su, Ning, 2019, computer code simpleboot, https://gitlab.com/bootstrapcollaboration/simpleboot.

Su, Ning, 2020, letter to Slava Rychkov (March 7, 2020).

Su, Ning, 2022a, "Skydiving to bootstrap islands: An algorithm for dynamically constrained SDP," lecture, 2022 Simons Collaboration on the Nonperturbative Bootstrap Annual Meeting, 2022, https://www.simonsfoundation.org/event/simons-collaboration-on-the-nonperturbative-bootstrap-annual-meeting-2022/.

Su, Ning, 2022b, "The hybrid bootstrap," arXiv:2202.07607.

Su, Ning, 2023, "Semidefinite program and the navigator function," lecture, Mini-Course of Numerical Conformal Bootstrap, 2023, https://pirsa.org/23040145.

Takahashi, Jun, Hui Shao, Bowen Zhao, Wenan Guo, and Anders W. Sandvik, 2024, "SO(5) multicriticality in two-dimensional quantum magnets," arXiv:2405.06607.

Wikipedia, 2024a, "Delaunay triangulation," https://en.wikipedia.org/wiki/Delaunay_triangulation.

Wikipedia, 2024b, "Broyden-Fletcher-Goldfarb-Shanno algorithm," https://en.wikipedia.org/wiki/Broyden-Fletcher-Goldfarb-Shanno_algorithm.

Wilson, Kenneth G., 1969, “Non-Lagrangian models of current algebra,” Phys. Rev. **179**, 1499–1512.

Xu, Cenke, and Yi-Zhuang You, 2015, “Self-dual quantum electrodynamics as boundary state of the three-dimensional bosonic topological insulator,” Phys. Rev. B **92**, 220416.

Zerf, Nikolai, Luminita N. Mihaila, Peter Marquard, Igor F. Herbut, and Michael M. Scherer, 2017, “Four-loop critical exponents for the Gross-Neveu-Yukawa models,” Phys. Rev. D **96**, 096010.

Zhou, Zheng, Liangdong Hu, W. Zhu, and Yin-Chen He, 2024, “SO(5) Deconfined Phase Transition under the Fuzzy-Sphere Microscope: Approximate Conformal Symmetry, Pseudo-Criticality, and Operator Spectrum,” Phys. Rev. X **14**, 021044.

Zhu, Wei, Chao Han, Emilie Huffman, Johannes S. Hofmann, and Yin-Chen He, 2023, “Uncovering Conformal Symmetry in the 3D Ising Transition: State-Operator Correspondence from a Quantum Fuzzy Sphere Regularization,” Phys. Rev. X **13**, 021009.